Article

Molecular Cell

Conversion of Bim-BH3 from Activator to Inhibitor of Bak through Structure-Based Design

Graphical Abstract

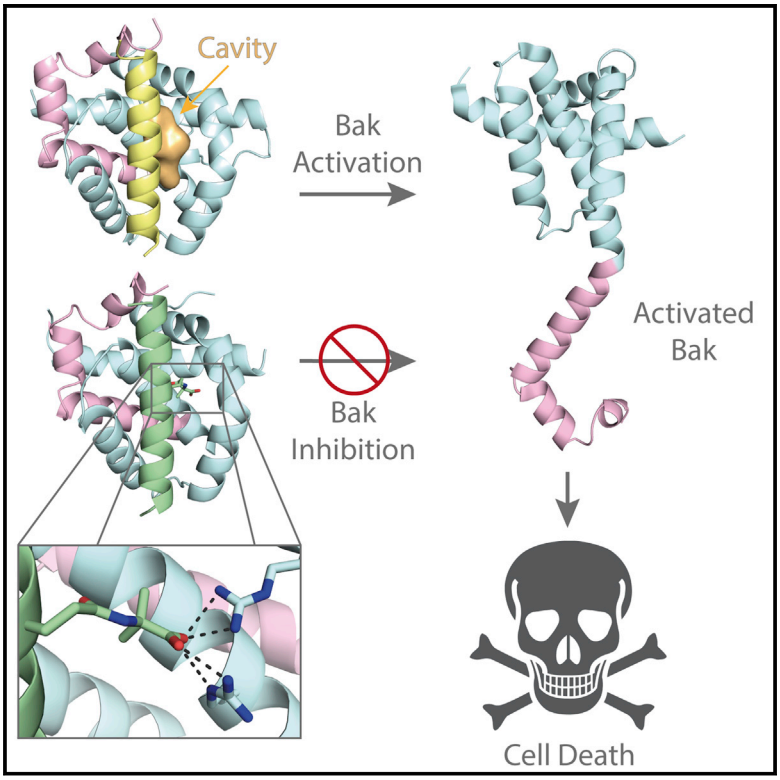

Authors

Jason M. Brouwer, Ping Lan, Angus D. Cowan, ..., Guillaume Lessene, Peter M. Colman, Peter E. Czabotar

Correspondence

czabotar@wehi.edu.au

In Brief

Brouwer et al. describe the first crystal structures of BH3-only peptides bound to Bak, which reveal a cavity that may be important for activation. They then use structure-based design to alter the Bim-BH3 peptide and convert it from an activator to an inhibitor of Bak.

Highlights

- First crystal structure of Bak bound to a BH3-only peptide
- First inhibitor of Bak with a clearly defined molecular mechanism
- BH3 binding is sufficient to disrupt Bak from the complex containing VDAC2
- Ligands that form a stable complex with Bak can block its activation

Brouwer et al., 2017, Molecular Cell *68*, 659–672
November 16, 2017
https://doi.org/10.1016/j.molcel.2017.11.001

Molecular Cell
Article

Conversion of Bim-BH3 from Activator to Inhibitor of Bak through Structure-Based Design

Jason M. Brouwer,[1,2] Ping Lan,[1,2] Angus D. Cowan,[1,2] Jonathan P. Bernardini,[1,2] Richard W. Birkinshaw,[1,2] Mark F. van Delft,[1,2] Brad E. Sleebs,[1,2] Adeline Y. Robin,[1,2] Ahmad Wardak,[1] Iris K. Tan,[1] Boris Reljic,[1,2] Erinna F. Lee,[4,5,6] W. Douglas Fairlie,[4,5,6] Melissa J. Call,[1,2] Brian J. Smith,[4] Grant Dewson,[1,2] Guillaume Lessene,[1,2,3,7] Peter M. Colman,[1,2,7] and Peter E. Czabotar[1,2,7,8,*]

[1]Walter and Eliza Hall Institute of Medical Research, 1G Royal Parade, Parkville, VIC 3052, Australia
[2]Department of Medical Biology, The University of Melbourne, Melbourne, VIC 3052, Australia
[3]Department of Pharmacology and Therapeutics, The University of Melbourne, Melbourne, VIC 3052, Australia
[4]La Trobe Institute for Molecular Sciences, La Trobe University, Melbourne, VIC 3086, Australia
[5]Olivia Newton-John Cancer Research Institute, Heidelberg, VIC 3084, Australia
[6]School of Cancer Medicine, La Trobe University, Melbourne, VIC 3086, Australia
[7]Senior Author
[8]Lead Contact
*Correspondence: czabotar@wehi.edu.au
https://doi.org/10.1016/j.molcel.2017.11.001

SUMMARY

Certain BH3-only proteins transiently bind and activate Bak and Bax, initiating their oligomerization and the permeabilization of the mitochondrial outer membrane, a pivotal step in the mitochondrial pathway to apoptosis. Here we describe the first crystal structures of an activator BH3 peptide bound to Bak and illustrate their use in the design of BH3 derivatives capable of inhibiting human Bak on mitochondria. These BH3 derivatives compete for the activation site at the canonical groove, are the first engineered inhibitors of Bak activation, and support the role of key conformational transitions associated with Bak activation.

INTRODUCTION

Programmed cell death, or apoptosis, is a biological process crucial for embryonic development and tissue homeostasis. Apoptotic malfunction contributes to a number of disease states. Insufficient apoptosis is a hallmark of cancer (Hanahan and Weinberg, 2011), and excessive apoptosis has been implicated in the pathology of a variety of conditions including neurodegenerative disorders (Wiessner et al., 1999), heart attack (Dorn, 2009), stroke (Rami et al., 2008), retinal degeneration (Remé et al., 2000), hearing loss (Someya and Prolla, 2010), and traumatic brain injury (Tehranian et al., 2008).

Interactions between members of the Bcl-2 family of proteins govern the mitochondrial pathway to apoptosis. The family is comprised of sensors (BH3-only proteins), effectors (Bak and Bax and perhaps Bok), and inhibitors (pro-survival proteins including Bcl-2 itself) (Adams and Cory, 1998). In response to apoptotic stimuli, BH3-only proteins may be cleaved (Li et al., 1998; Luo et al., 1998; Yin et al., 1999), undergo translocation (Puthalakath et al., 1999), undergo phosphorylation (Zha et al., 1996), or be upregulated (Nakano and Vousden, 2001; Yu et al., 2001) to induce apoptosis. Certain BH3-only proteins (direct activators, e.g., Bim, Bid, Puma, and possibly Noxa) can directly activate Bak and Bax, leading to oligomers of these proteins that cause irreversible mitochondrial outer membrane permeabilization (MOMP) (Dai et al., 2011, 2014; Kuwana et al., 2005; Letai et al., 2002; Lindsten et al., 2000; Wei et al., 2000, 2001). MOMP results in the release of cytochrome *c* (Kluck et al., 1997; Liu et al., 1996) and other apoptogenic factors that initiate caspase activation and ultimately the demolition of the cell. Pro-survival proteins prevent cell death either by binding activated Bak/Bax (Czabotar et al., 2011; Ku et al., 2011; Lee et al., 2016; Llambi et al., 2011; Willis et al., 2005) or by binding BH3-only proteins capable of activating Bak/Bax (Certo et al., 2006; Letai et al., 2002). Other BH3-only proteins (indirect activators, e.g., Bad, Bmf, Bik, and Hrk) promote apoptosis by competing for binding to the pro-survival proteins, thereby liberating direct activator BH3-only proteins and/or activated Bak and Bax molecules (Hockings et al., 2015; Letai et al., 2002; Llambi et al., 2011).

Activation of Bak and Bax results in a series of conformational changes including dissociation of the α1 helix (Griffiths et al., 1999; Hsu and Youle, 1997), BH3-domain exposure (Dewson et al., 2008), and the release of their core domains (α2–α5) from their latch domains (α6–α8) (Brouwer et al., 2014; Czabotar et al., 2013). Freed core domains form symmetric dimers in which α2 (the BH3) of one polypeptide engages α3, α4, and α5 (the groove) of the other. These BH3-in-groove homodimers are the building block of membrane permeabilizing oligomers (Aluvila et al., 2014; Bleicken et al., 2010, 2014; Brouwer et al., 2014; Czabotar et al., 2013; Dewson et al., 2008, 2012; Subburaj et al., 2015). An important feature of this model is that in order for the core domains to dimerize, the BH3 activator must first disengage to liberate the interface (α3, α4, α5) utilized in the BH3-in-groove homodimer. Structural studies have revealed how BH3-only proteins directly engage with the hydrophobic

groove of Bax. These interactions result in the formation of a cavity within the complex, which may contribute to its destabilization and facilitate the conformational changes that occur during activation (Czabotar et al., 2013). BH3-only proteins activate Bak in a similar manner to Bax, by engaging the hydrophobic groove (Leshchiner et al., 2013). An NMR structure of Bak in complex with a stapled Bid-BH3 peptide provided the first structural details of such an interaction (Moldoveanu et al., 2013), but revealed no potential cavities as observed in the Bax crystal structures.

There are no reported specific inhibitors of Bak. Although inhibitors of Bax-mediated cell death have previously been identified from phenotypic screens (Bombrun et al., 2003; Brahmbhatt et al., 2016; Hetz et al., 2005; Jiang et al., 2007; Peixoto et al., 2017; Polster et al., 2003), most of these compounds are very hydrophobic, and their direct interaction with Bax has not been demonstrated. It remains possible that they act through perturbation of the mitochondrial outer membrane rather than specifically inhibiting Bax. Recently developed inhibitors that are thought to disrupt oligomerization of both Bak and Bax were observed to decrease chemical cross-linking on α6 and α9 helices and some parts of the BH3-in-groove interaction (Niu et al., 2017). However, at high concentrations they cause morphological alterations in cells, so their mode of action is unclear.

Here we describe the first rationally designed Bak inhibitory peptide with a defined mechanism of action. Discovery of this molecule was initiated by solving the first crystal structures of a BH3-peptide (Bim-BH3) bound to Bak. A cavity is present in these complexes, although in a different position from that seen in Bax structures, and is filled with solvent components. From these crystal structures, we engineered a high-affinity Bim-like peptide, incorporating a non-natural amino acid that switches the peptide from being an activator of Bak to being an inhibitor of Bak. Further structure-guided changes to this inhibitor resulted in an agent capable of blocking Bak activation at the mitochondria. The data presented here provide the first evidence that a ligand forming a stable complex with Bak at the activation site can block apoptosis induction.

RESULTS

Crystal Structure of Bim-BH3 Bound to Bak

Recombinant human Bak (hBak; ΔN22, ΔC25, C166S) forms core/latch dimers in the presence of Bid-BH3 peptide and the detergent CHAPS (Brouwer et al., 2014). hBak core/latch dimers were produced using the method reported in Brouwer et al. (2014), then reconstituted with a 5-fold molar excess of a mutant Bim-BH3 peptide (Bim-RT that contains the mutations W147R and Y163T, to increase solubility and reduce the propensity of the Bim-WT [wild-type] peptide to crystallize on its own [Robin et al., 2015]). Two independent crystal structures were solved (Figures 1A and S1A, Table 1); both reveal a core/latch dimer in complex with a Bim-RT peptide bound at each canonical BH3-binding site. Aside from high B-factors for one-half of the dimer in the tetragonal form (Figure S1B), the two crystal structures show only minor differences in the α2–α3 helix corner (Figure S1C). The α1–α2 loop could be completely built in the cubic space group, showing for the first time in either Bak (Brouwer et al., 2014) or Bax (Czabotar et al., 2013) that the α1 helix remains with the "core" and is not also "domain-swapped" like the α6–α8 in the core/latch dimer (Figure 1A). Bim-RT binds to the canonical (α3, α4, and α5) hydrophobic groove of Bak primarily through hydrophobic moieties (h0–h4) and a conserved salt bridge (Bim-D157: Bak-R127) (Figure 1B). R153 on Bim-RT is hydrogen bonded to the carbonyl group of S117 on the α4 backbone of Bak (Figure 1B) in a manner similar to that previously observed in the Bax:Bim-BH3 structure (Robin et al., 2015). Differences in the structure of the groove between the apo-Bak and peptide-bound-Bak complexes are most notable at helices α2 and α3 (Figure S1D). The Bim-BH3 peptides in both crystal structures are helical throughout compared to the previously solved Bid-BH3 NMR structure (Figure S1E).

We observed a cavity in the Bak:Bim-RT complex structures (Figures 1C and S1F) that is not evident in the Bak:Bid-BH3 NMR structure (PDB: 2M5B) or apo-Bak crystal structures (PDB: 2IMS, 2IMT, 2YV6, 4U2U). The cavity is located between the Bim-RT peptide and the α1, α2, α3, and α5 helices. In the cubic crystal structure, this cavity is approximately 435 $Å^3$ and possesses density consistent with one molecule of TFA (trifluoroacetic acid) (Figure 1D) and several water molecules. A composite omit map generated after the final build also shows clear density for a TFA molecule (Figure 1E). The cavity in the tetragonal crystal structure is 351 $Å^3$ and likely occupied by an MPD (2-methyl-2,4-pentanediol) and water molecules (Figure S1G). TFA and MPD make hydrogen bonds with R42 (α1) and R137 (α5) in Bak. The MPD molecule was present in the crystallization condition for the tetragonal space group, and the TFA in the cubic structure was likely derived from synthesis of the Bim-RT peptide and co-purified with the complex. The different cavity sizes in the two Bak:Bim-BH3 crystal structures may be due to different crystal contacts around the α2 and α3 helices or simply due to the different molecules trapped in them.

why is there a cavity?

Evidently, Bak core/latch dimers are able to bind native Bim-BH3 peptides to form complexes sufficiently stable for structural studies, while monomeric Bak cannot. A possible structural basis for this anomaly may lie in the conformation of L100 in the Bak monomer versus core/latch dimer structures. Four crystal structures of monomeric Bak have been solved (PDB: 2IMS, 2IMT, 2JCN, 2YV6) (Moldoveanu et al., 2006; Wang et al., 2009). The α3–α4 loop adopts different conformations in these structures. In 2IMS and 2IMT, L100 is shielded from solvent by Y110, whereas in PDB: 2JCN and PDB: 2YV6, α3 is extended by one helical turn (possibly due to crystal contacts) and L100 is solvent exposed (Figure S2A). The core/latch dimer structure of apo-Bak (PDB: 4U2U) shows L100 in the solvent-exposed conformation, apparently "ready" for engaging the Bim-BH3 peptide as seen in the new structure described here (Figure S2B). In this position L100 contributes to the "p0" pocket that engages the "h0" amino acids of the BH3 peptide (Figure 2A), an interaction we have previously shown to be critical for BH3 peptides to activate Bax (Czabotar et al., 2013) and Bak (Brouwer et al., 2014). In order to investigate the importance of the L100 to BH3-peptide binding, we mutated the residue to an alanine. Dimerization of recombinant Bak L100A by Bid-BH3 (Figure S2C) was significantly reduced

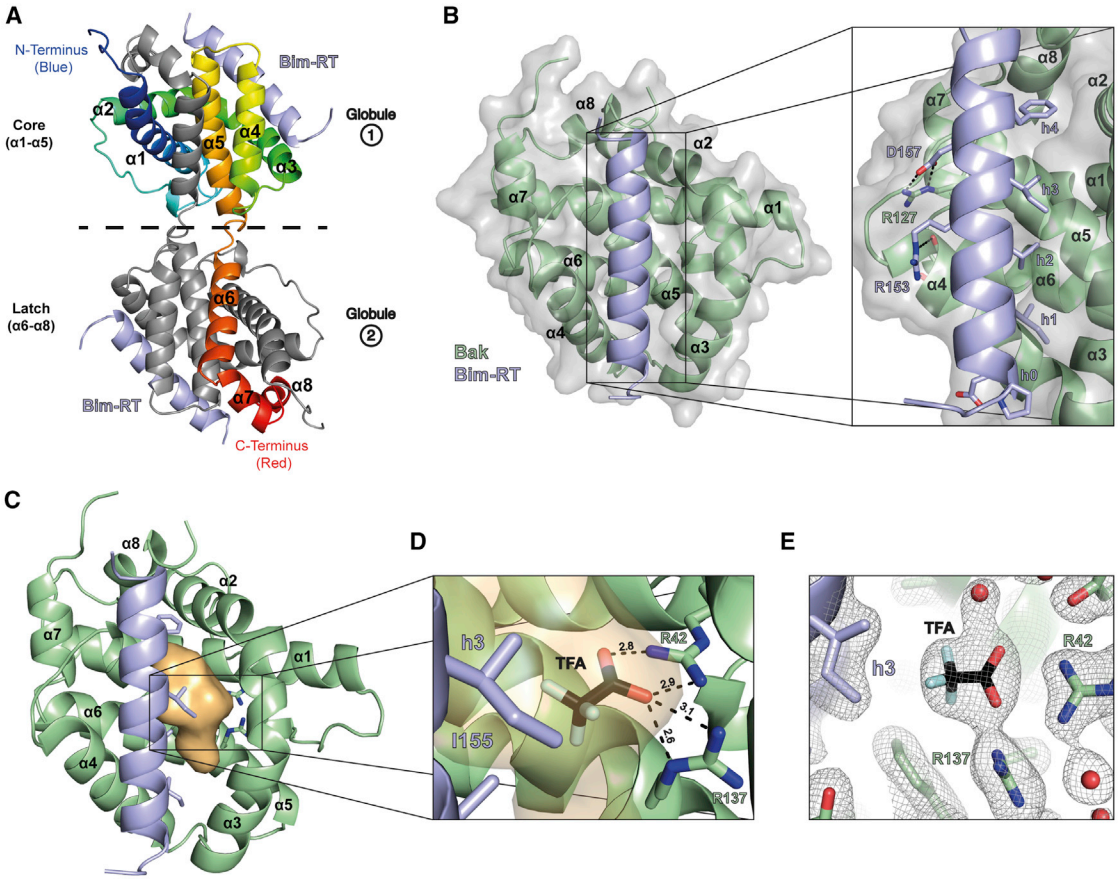

Figure 1. Crystal Structure of Bim-BH3-RT Bound to Bak

(A) Crystal structure (cubic space group) of the Bak core/latch dimer bound to Bim-RT. One molecule of Bak is colored rainbow from N (blue) to C terminus (red); the other polypeptide is colored gray. Bim-RT (pale blue) binds to both globules of the dimer at each hydrophobic groove (α2–α5).

(B) One globule of the Bak core/latch dimer (cartoon, green; surface, gray) bound to Bim-RT (pale blue). Bim interacts with Bak via hydrophobic moieties h0–h4, a salt bridge (Bim-D157: Bak-R127), and other hydrogen-bonding interactions (e.g., Bim-R153: α4 helix backbone of Bak).

(C) Bim-RT binding induced the formation of a cavity (orange surface) in Bak with a volume of ~435 Å^3.

(D) A TFA molecule could be refined in the cavity shown in (C); TFA interacts with R42 (α1 helix) and R137 (α5 helix) of Bak through charge-charge interactions. The TFA molecule resides proximal to the h3 position (I155) of the Bim peptide (pale blue). Bond distances in Å are shown with black dashed lines.

(E) A composite omit map ($2mF_o$-DF_c, σ = 1.5) of the Bak:Bim-RT cubic structure showing clear density for the TFA molecule.

See also Figures S1 and S2 and Table 1.

compared to the wild-type protein (Brouwer et al., 2014), and the L100A mutation severely impaired Bak-mediated permeabilization of liposomes induced by both Bid-BH3 and Bim-RT (Figures S2D and S2E). Interestingly, increasing the concentration of Bid-BH3 100-fold could compensate for the impaired function of L100A mutant on liposomes (Figure S2F). We solved the crystal structure of Bak L100A (Figure S2G, Table 1), showing that A100 is solvent exposed like L100 in the core/latch dimer (PDB: 4U2U), but unlike L100 in monomeric Bak (PDB: 2IMS). Nevertheless, the additional hydrophobicity of L100 appears to be required for engaging BH3 peptides, further confirming the role for the h0:p0 interaction in Bak activation.

Bim-h3Pc, an Engineered Bim-BH3 that Specifically Inhibits Bak Activation

The TFA molecule observed in the Bak:Bim-RT crystal structure is adjacent to I155 at the h3 position of the Bim-RT peptide (Figures 1D and 2A). We hypothesized that a peptide with an artificial amino acid capable of mimicking the charge-charge interactions present between the TFA molecule and R42/R137 of hBak would have increased affinity for Bak. Modeling suggested that a pentyl-carboxylate residue would satisfy this requirement. The derivative peptide, Bim-h3Pc-RT (Figure 2A), displays markedly different binding kinetics to hBak as compared with Bim-WT (Figures 2B and 2C) (for characterization of non-natural amino acids and peptides containing non-natural amino acids, refer to Data S1). These surface plasmon resonance (SPR) experiments showed decreased on and off rates for Bim-h3Pc-RT, allowing their determination by fitting to a 1:1 binding model yielding a dissociation constant (KD) of 1.3 ± 0.5 μM (SD, n = 3). It was not possible to calculate a KD for Bim-WT from this experiment due to fast on and off rates and sub-saturating responses at steady state (Figure S3A).

Table 1. Data Collection and Refinement Statistics for Bak:Bim-RT, Bak L100A, Bak:Bim-h3Pc, and Bak:Bim-h3Pc-RT

	Bak Core/Latch Dimer: Bim-RT (Cubic) (PDB: 5VWV)	Bak Core/Latch Dimer: Bim-RT (Tetragonal) (PDB: 5VWW)	Bak L100A (PDB: 5VX1)	Bak Monomer: Bim-h3Pc (PDB: 5VWZ)	Bak Core/Latch Dimer: Bim-h3Pc-RT (PDB: 5VWY)
Data Collection					
Space group	$P4_132$	$P4_32_12$	$P2_1$	$P2_1$	C2
Unit Cell					
a, b, c (Å)	139.40, 139.40, 139.40	87.79, 87.79, 95.46	41.50, 39.49, 108.11	38.24, 56.67, 79.29	65.89, 37.54, 69.56
α, β, γ (°)	90, 90, 90	90, 90, 90	90, 91.255, 90	90, 103.32, 90	90, 107.858, 90
Wavelength (Å)	0.9537	0.9537	0.9537	0.9537	0.9537
Resolution range (Å)	42.02–1.90 (1.97–1.90)	43.9–2.8 (2.90–2.80)	36.03–1.22 (1.27–1.22)	38.58–1.62 (1.68–1.62)	32.45–1.56 (1.61–1.56)
R_{merge}	0.2162 (3.84)	0.1196 (1.851)	0.04585 (0.6494)	0.1174 (0.848)	0.06555 (0.6122)
I/σ(I)	24.26 (1.48)	19.77 (1.51)	14.94 (1.97)	15.10 (2.67)	13.68 (1.49)
Completeness (%)	100.00 (100.00)	1.00 (0.99)	0.95 (0.91)	1.00 (0.99)	0.93 (0.67)
Multiplicity	47.8 (47.0)	14.0 (13.5)	3.8 (3.8)	7.4 (7.2)	3.6 (2.5)
CC 1/2	0.999 (0.497)	0.999 (0.498)	0.999 (0.687)	0.998 (0.764)	0.999 (0.637)
Refinement					
Resolution range (Å)	42.02–1.90 (1.97–1.90)	43.9–2.8 (2.90–2.80)	36.03–1.22 (1.27–1.22)	38.58–1.62 (1.68–1.62)	32.45–1.56 (1.61–1.56)
Total reflections	1,777,017 (170,641)	134,193 (12,283)	370,023 (35,493)	311,133 (29,715)	79,509 (3,880)
Unique reflections	37,154 (3,647)	9,619 (910)	98,200 (9,381)	41,869 (4,133)	21,929 (1,567)
R-work	0.1568 (0.2823)	0.2180 (0.2989)	0.1681 (0.2659)	0.1547 (0.2225)	0.1761 (0.3473)
R-free	0.1771 (0.2912)	0.2744 (0.3138)	0.1889 (0.2805)	0.1886 (0.2848)	0.2165 (0.3984)
Number of Atoms					
Protein/Peptide	1,560	2,744	2,886	3,168	1,454
Ligands	38	15	0	52	17
Solvent	185	18	480	390	138
Average B-Factor					
Protein/Peptide	38.58	119.69	22.40	20.02	26.31
Ligands	70.32	83.41	n/a	30.94	18.29
Solvent	51.87	64.50	35.61	29.24	38.31
Root-Mean-Square Deviations					
Bond lengths (Å)	0.007	0.002	0.014	0.006	0.006
Bond angles (°)	0.76	0.33	1.44	0.79	0.76
Ramachandran					
Favored (%)	99	98	98	99	98
Outliers (%)	0	0	0.56	0.26	1.2

Numbers in parentheses refer to outer-shell statistics.

Previously, we have shown that BH3-peptides capable of inducing core/latch dimers in the presence of CHAPS are activators of Bak (Brouwer et al., 2014) (Figure 2D). In contrast, Bim-h3Pc-RT peptide did not induce Bak dimerization (Figure 2D). A subtle shift in the gel filtration elution profile was also observed in the Bak:Bim-h3Pc-RT peak, suggesting a stable complex had formed even in the absence of CHAPS (Figure 2D). Bim-h3Pc-RT was also incubated with recombinant Bak and then challenged with Bid-BH3 peptide (the most potent BH3-peptide activator of Bak in this assay); under these conditions Bim-h3Pc-RT completely inhibited Bid-BH3-induced dimerization of Bak as analyzed by gel filtration (Figure 2E). Bim-RT, itself a weak activator of Bak, was unable to inhibit Bid-BH3-induced dimerization of Bak, demonstrating the importance of the pentyl-carboxylate side chain for inhibition (Figure S3B).

Bim-h3Pc-RT peptides bound to Bak with a higher affinity, yet did not activate the protein. Liposome release assays were used to test whether Bim-h3Pc-RT could inhibit Bak permeabilization of membranes. hBak with a C-terminal His-tag was added to Ni-liposomes and then pre-treated with varying concentrations of Bim-h3Pc-RT before being activated by Bid-BH3 peptide.

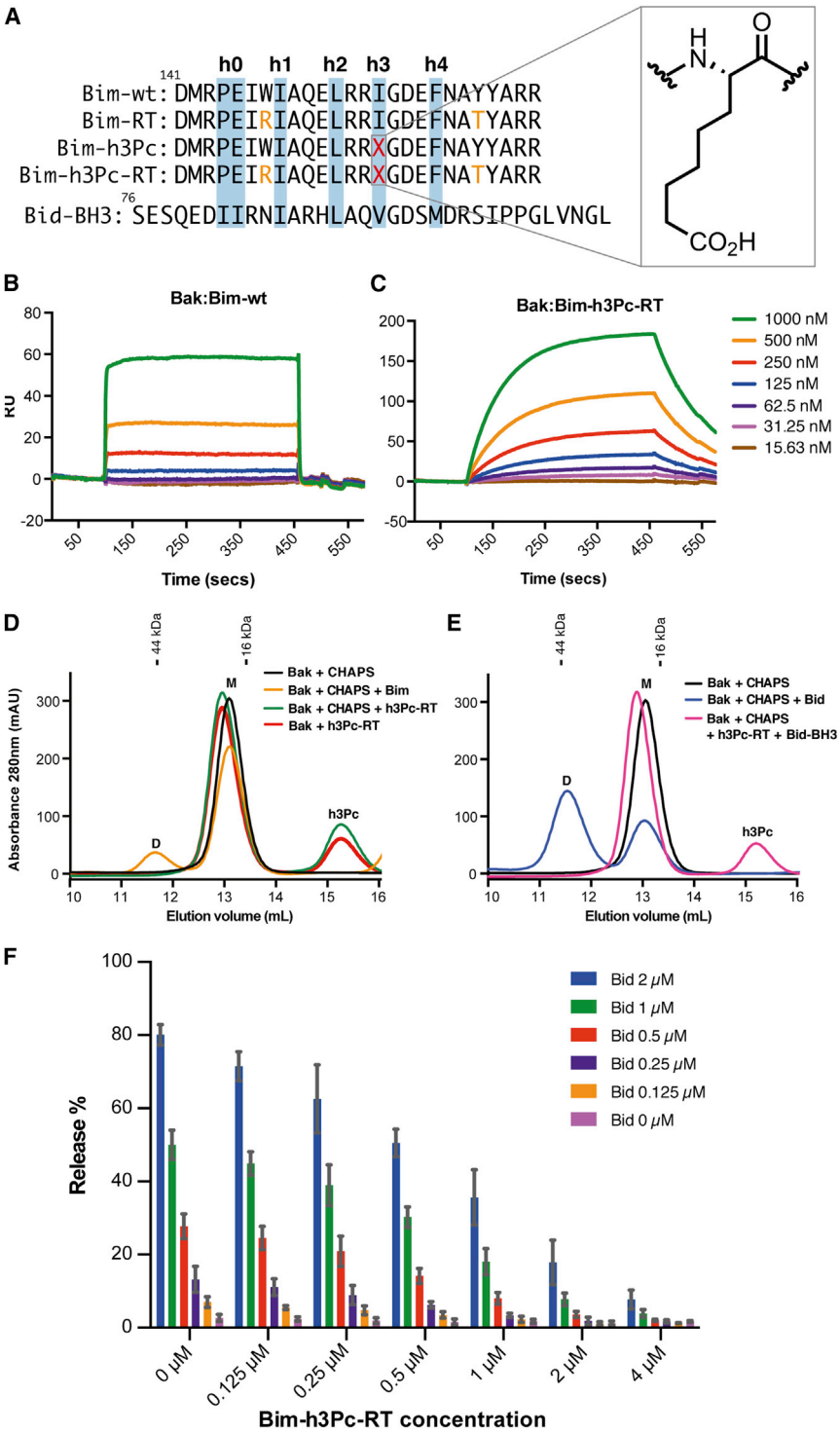

Figure 2. Bim-h3Pc-RT Inhibits Human Bak Activation

(A) Sequence of wild-type (WT) Bim-WT, Bid-BH3, and Bim-RT that contain hydrophobicity-reducing mutations (orange, W147R and Y163T) and Bim-h3Pc and Bim-h3Pc-RT with moieties previously found to be important for interactions between BH3-only proteins and Bak/Bax highlighted (h0–h4) (Czabotar et al., 2013; Brouwer et al., 2014; Robin et al., 2015). The chemical structure of the non-natural amino acid pentyl-carboxylate is shown and labeled X at the h3 position (red) in the sequence.

(B and C) Surface plasmon resonance sensorgrams for the direct binding of varying concentrations of Bim-WT or Bim-h3Pc-RT, respectively, to Bak. Bak:Bim-WT binding displayed fast on and off rates that were not possible to fit to a kinetic binding model and did not achieve saturation required for steady-state analysis. Bim-h3Pc-RT bound to Bak with a KD of 1.3 ± 0.5 μM (n = 3, SD).

(D) Bak (100 μM) in the presence of CHAPS (black) elutes as a monomer (M) on gel filtration (S75 10/300) and can be dimerized (D) with the addition of Bim-WT (1 mM) peptide (orange). Bim-h3Pc-RT (1 mM) ± CHAPS (green, red) did not dimerize Bak, but eluted slightly earlier, suggesting a Bak:h3Pc complex had formed.

(E) The activating peptide Bid-BH3 (1 mM) dimerizes Bak (100 μM) in the presence of CHAPS (blue) as analyzed by gel filtration (S75 10/300). When Bak (100 μM) was pre-incubated with Bim-h3Pc-RT (1 mM) and CHAPS and then challenged with Bid-BH3 (1 mM), dimerization was blocked. Bak (100 μM) monomer plus CHAPS is colored black and shown as a reference. Gel filtration experiments in (D) and (E) are representative of three independent experiments.

(F) Liposomes with encapsulated self-quenching fluorescent dye were pre-incubated with Bak and varying concentrations of Bim-h3Pc-RT peptide. They were then challenged with up to 2 μM Bid-BH3 as an activation stimulus. Release was normalized to detergent-solubilized liposomes. Increasing the Bim-h3Pc-RT concentration led to a reduction in fluorescent dye release, consistent with inhibition of membrane permeabilization (n = 3, mean ± SEM). See also Figures S3 and S1.

We observed decreasing liposome permeabilization with increasing concentrations of Bim-h3Pc-RT (Figure 2F). IC_{50} values for inhibition of 2 μM and 1 μM Bid-BH3 are 880 nM and 700 nM, respectively (Figure S3C), consistent with the binding affinity from Biacore analyses. Inhibition was specific for hBak as Bim-h3Pc-RT was not capable of inhibiting mouse Bak (mBak), in which the equivalent amino acid to R42 is L40, or human Bax (hBax) on liposomes (Figures S3D and S3E). Bax has charged residues (R34 and K119) at similar positions to those of hBak (R42 and R137) that could conceivably also bind the Bim-h3Pc-RT peptide. However, Bax has a large residue at the location occupied by the pentyl-carboxylate of the peptide (Y115, corresponding to hBak G133) that would prevent binding of this moiety (Figure S3F).

Purified monomeric Bak and Bak core/latch dimers were crystalized in a 4-fold molar excess of either Bim-h3Pc or

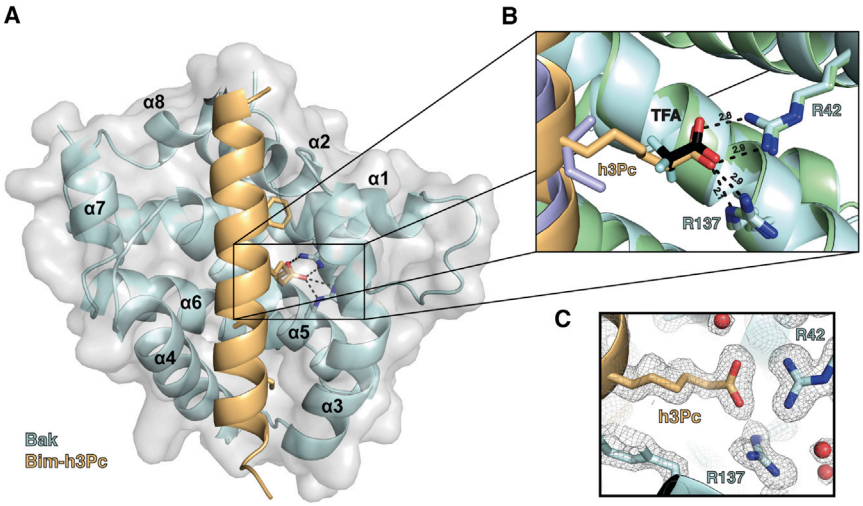

Figure 3. Crystal Structure of Bim-h3Pc Bound to Bak

(A) Crystal structure of Bim-h3Pc (pale orange) bound to the hydrophobic groove of Bak (ΔN22, ΔC25, ΔCys) (cartoon, pale cyan; surface, gray).

(B) Overlay of Bak:Bim-RT (Bim, pale blue; Bak, pale green) and Bak:Bim-h3Pc crystal structures. The TFA molecule from the Bak:Bim-RT structure interacts with R42 and R137 of Bak, analogous to the pentyl-carboxylate residue in the Bak:Bim-h3Pc structure. Bond distances in Å are shown in black dashed lines.

(C) Composite omit map ($2mF_o$-DF_c, σ = 1.5) showing unbiased density for the pentyl-carboxylate side chain in the Bak:Bim-h3Pc crystal structure. See also Figure S4 and Table 1.

Bim-h3Pc-RT, respectively, and crystal structures of both were solved (Figures 3A, S4A, and S4B, Table 1). The increased affinity of Bim-h3Pc for Bak and its failure to activate Bak facilitated the capture of a crystal structure of the complex with monomeric Bak. In both structures the pentyl-carboxylate residue enters the p3 pocket in the canonical groove of Bak, displaces solvent molecules, and interacts with R42 and R137, mimicking the binding mode of the TFA molecule and its interactions with these residues in the Bim-Bim-RT:Bak structure (Figures 3B and 3C). These additional interactions within the core of the protein provide a rationale for the slower on and off rates for Bim-h3Pc peptide to Bak compared to Bim-WT.

Bim-h3Pc Retains High Affinity for Mcl-1 and Bcl-x_L

Bim-h3Pc-RT was tested for its capacity to inhibit Bak activation on isolated mitochondria from *Bak*$^{-/-}$*Bax*$^{-/-}$ double knockout (DKO) mouse embryonic fibroblasts (MEFs) reconstituted with hBak. Bim-h3Pc-RT did not inhibit cytochrome *c* release induced by Bid-BH3, but instead initiated release of cytochrome *c* (Figure 4A). We hypothesized this may be due to retained binding affinity for pro-survival proteins. The Bim-h3Pc-RT peptide bound to Mcl-1 and Bcl-x_L, the two prominent pro-survival proteins inhibiting Bak activity in MEFs (Willis et al., 2005), with nanomolar affinity (Figure 4B, Table S1), as previously reported for Bim-BH3 (Chen et al., 2005). We also solved crystal structures of Bcl-x_L and Mcl-1 bound to Bim-h3Pc-RT (Figure 4C, Table 2). In both cases the flexibility of the charged pentyl-carboxylate side chain enables it to snake out of the shallow p3 pockets present in complexes of Mcl-1 and Bcl-x_L with BH3 ligands (Figure 4C). Interactions of the Bim-h3Pc-RT peptide are very similar to those previously observed for Bim-BH3 bound to Mcl-1 (PDB: 2NL9) (Czabotar et al., 2007) and Bcl-x_L (PDB: 3FDL) (Lee et al., 2009), with the only major differences being the h3 residue itself (Figures S5A and S5B).

Inhibition of Mitochondrial Bak

To overcome binding to pro-survival proteins at the mitochondria, alterations were made to the pentyl-carboxylate in Bim-h3Pc-RT. Molecular modeling was used to estimate binding capacities of a variety of alternate side chains, the best scoring of which was Bim-h3Glg ($PLANTS_{PLP}$ docking score = −120) (Figure S6A). The Glg and a related side chain Glt were then chemically synthesized (Figure S6B) and incorporated into the Bim-RT peptide sequence (Figure 5A). The h0 position in Bid is known to be important for Bak activation (Brouwer et al., 2014; Hockings et al., 2015). A version of Bim-h3Glt with the h0 residues of Bid (P144I, E145I) and several other mutations introduced to aid solubility (M142S, I146S, W147R, Y162T) was also synthesized (Bim-h0-h3Glt) (Figure 5A).

SPR was used to analyze binding of these new inhibitor peptides to Bak, Mcl-1, and Bcl-x_L (Table S1). Bim-h3Glg showed reduced affinity for Bak (KD = 21 ± 3 μM) and significantly weaker affinity for Mcl-1 (KD = 410 ± 70 nM), yet retained low nM binding for Bcl-x_L (KD = 1.9 ± 0.4 nM) (Figure 5B). Bim-h3Glt exhibited affinity for Bak (KD = 1.0 ± 0.1 μM) comparable to the original peptide Bim-h3Pc-RT and a weaker interaction with Mcl-1 (KD = 300 ± 20 nM), yet still bound Bcl-x_L with high affinity (KD = 4.2 ± 0.7 nM) (Figure 5B). The addition of two isoleucine residues into the h0 position of the Bim-h3Glt peptide (Bim-h0-h3Glt) provided a ~65-fold increase in affinity for Bak (KD = 14.9 ± 0.3 nM) and resulted in a peptide that bound Bak more tightly than Mcl-1 (KD = 80 ± 11 nM) and similar affinity, despite striking differences in kinetics, to Bcl-x_L (KD = 21 ± 5 nM) (Figure 5B).

We solved the crystal structure of Bim-h0-h3Glt bound to Bak (Figure 5C, Table 2). The carboxylate moiety of the non-natural amino acid interacts with R42 and R137 (Figures 5C and S5C). The two isoleucine residues in the h0 moiety of the Bim-h0-h3Glt peptide straddle the Bak-L100 residue in the p0 pocket (Figure 5D). I144 interacts with L100 and the α3 helix where it is flanked by H99 ($p0_1$); I145 interacts with L100, Y110, and K113 ($p0_2$). Similar interactions are observed in the crystal structure of the core/latch dimer of Bax bound to the Bid BH3 peptide, where the key residue in the p0 pocket in Bax is V83 (Czabotar et al., 2013). These interactions explain the significant increase in affinity of Bim-h0-hGlt over Bim-h3Glt. The Bim-h0h3Glt peptide binds Bak L100A with 100-fold-lower affinity (KD = 1.5 ± 0.4 μM) (Figure S6D, Table S1) than Bak-WT. We

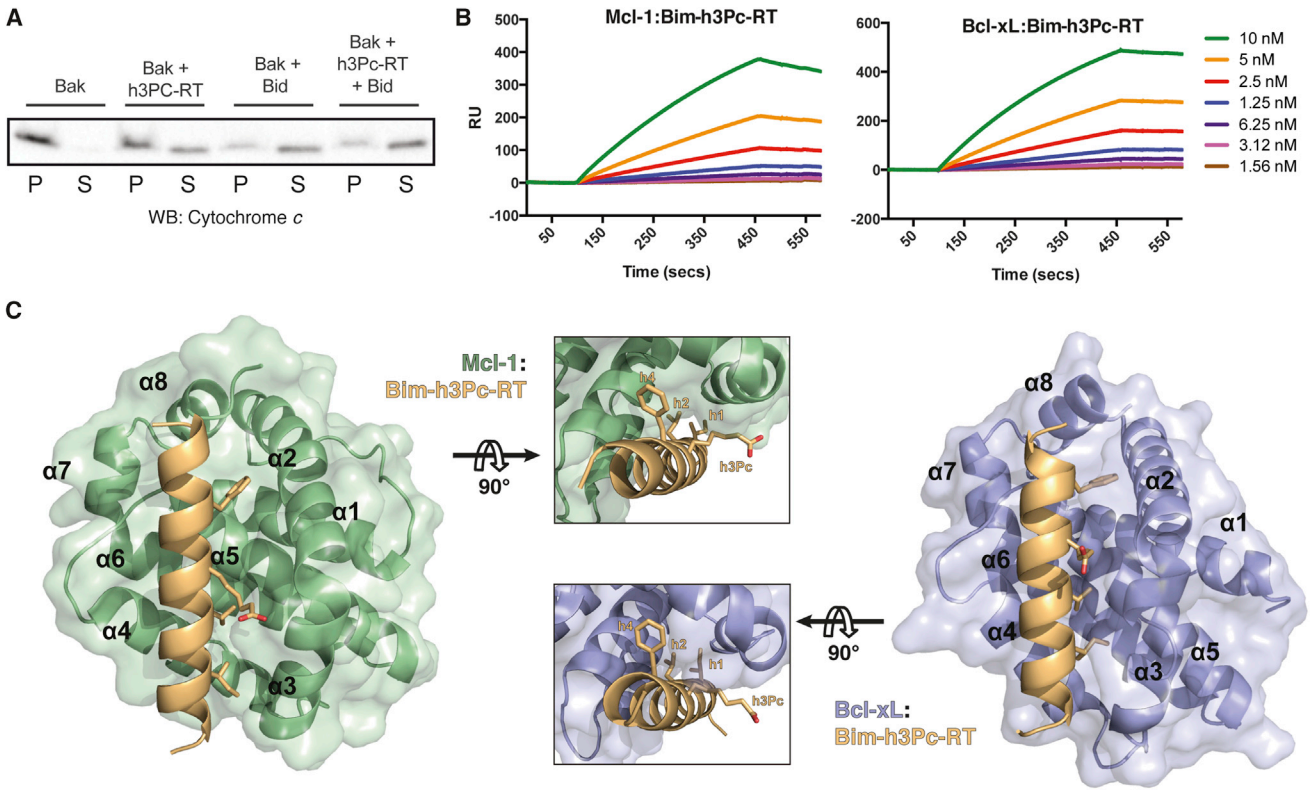

Figure 4. Bim-h3Pc-RT Binds Pro-survival Proteins Mcl-1 and Bcl-x_L with High Affinity

(A) Isolated mitochondria from DKO (*Bak*$^{-/-}$*Bax*$^{-/-}$) MEFs overexpressing human Bak were incubated with/without Bim-h3Pc-RT (5 μM) for 30 min and then treated with the activator stimulus Bid-BH3 (1.5 μM). Supernatant (S) and pellet (P) fractions were then analyzed by immunoblotting for cytochrome *c*. Release of cytochrome *c* from the pellet to the supernatant indicates Bak-mediated MOMP. Western blot is representative of three independent experiments.

(B) SPR binding curves for Mcl-1 and Bcl-x_L to immobilized Bim-h3Pc-RT. Mcl-1 binds to Bim-h3Pc-RT with a KD of 2.5 ± 3 nM (n = 3, SD) and to Bcl-x_L with a KD of 0.4 ± 0.4 nM (n = 3, SD).

(C) Crystal structure of Bim-h3Pc-RT (pale orange) bound to the hydrophobic groove of Mcl-1 (green surface and cartoon) and Bcl-x_L (blue surface and cartoon). The pentyl-carboxylate side chain is flexible and extruded from the hydrophobic groove when bound to Mcl-1 and Bcl-x_L (inset). See also Figure S5 and Tables 2 and S1.

also solved the crystal structure of the Bak:Bim-h3Glg complex (Table 2, Figures S6E and S6F), in which the Glg side chain binds in a similar manner to the Glt side chain and displays slight differences to the h3Pc side chain (Figure S6G).

The inhibitor peptide Bim-h0-h3Glt had both reduced affinity for Mcl-1 and Bcl-x_L and enhanced affinity for Bak, suggesting it might be capable of inhibiting Bak activation on mitochondria where pro-survival Bcl-2 proteins are also present. Mitochondria from *Bak*$^{-/-}$*Bax*$^{-/-}$ MEFs stably expressing hBak were incubated with Bim-h0-h3Glt, then challenged with Bid-BH3 peptide, and cytochrome *c* release was analyzed by western blot (Figure 5E). Consistent with its reduced affinity for pro-survival proteins, Bim-h0-h3Glt did not induce cytochrome *c* release (Figure 5E). Moreover, pre-incubation of mitochondria with 25 μM Bim-h0-h3Glt peptide blocked Bid-induced MOMP (Figure 5E). Addition of a mitochondrial targeting sequence (MTS) derived from Noxa (Seo et al., 2003) to the C terminus of the peptide (Bim-h0-h3Glt-MTS) increased potency of the inhibitor by approximately 50-fold in cytochrome *c* release assays (Figure 5F). The inhibitor peptide Bim-h0-h3Glt had no effect on mitochondria from *Bak*$^{-/-}$*Bax*$^{-/-}$ MEFs and failed to inhibit cytochrome *c* release when assayed on mitochondria expressing mBak (*Bax*$^{-/-}$ MEFs) (Figures S6H and S6I). Residue R42 on α1 of hBak is critical for Bim-h0-h3Glt function, as demonstrated by inhibition of cytochrome *c* release by Bim-h0-h3Glt from mitochondria expressing the mBak mutant L40R (Figure S6J). Bim-h0-h3Glt was also able to block indirect activation of Bak induced by the Mcl-1 inhibitor S63845 (Figure S6K) (Kotschy et al., 2016). Before activation, Bak associates with a high-molecular-weight complex that also contains VDAC2 (Figure S6L) (Lazarou et al., 2010). Once activated, Bak dissociates from this complex and forms BH3-in-groove dimers (Ma et al., 2013) (Figure 5G). Treatment with Bim-h0-h3Glt likewise induced Bak dissociation from the complex (Figure 5G), but blocked Bak activation, as measured by N-terminal epitope exposure, and dimerization (Figure 5G).

DISCUSSION

Characterizing the molecular details of how BH3-only proteins bind Bak and Bax is key to understanding how these critical effectors become activated to mediate apoptosis and also for

Table 2. Data Collection and Refinement Statistics for Crystal Structures of Bim-h3Pc-RT Bound to Mcl-1 and to Bcl-x_L, Bak:Bim-h0-h3Glt, and Bak:Bim-h3Glg

	Mcl-1: Bim-h3Pc-RT (PDB: 5VX2)	Bcl-xL: Bim-h3Pc-RT (PDB: 5VX3)	Bak Core/Latch Dimer: Bim-h0-h3Glt (PDB: 5VWX)	Bak Monomer: Bim-h3Glg (PDB: 5VX0)
Data Collection				
Space group	P 2_1	C2	P 2_1 2_1 2_1	P 2_1 2_1 2_1
Unit Cell				
a, b, c (Å)	42.03, 66.16, 76.67	125.66, 68.81, 102.83	61.63, 76.48, 77.55	48.09, 63.23, 121.04
α, β, γ (°)	90, 105.015, 90	90, 125.349, 90	90 90 90	90, 90, 90
Wavelength (Å)	0.9537	0.9537	0.9464	0.9537
Resolution range (Å)	32.25–1.85 (1.92–1.85)	41.41–1.95 (2.02–1.95)	48.25–2.49 (2.58–2.49)	44.69–1.60 (1.66–1.60)
R_{merge}	0.04656 (0.8135)	0.09715 (1.008)	0.1648 (0.757)	0.1559 (2.659)
I/σ(I)	15.79 (1.63)	8.40 (1.37)	8.51 (2.25)	11.78 (0.86)
Completeness (%)	0.99 (0.98)	0.99 (0.95)	0.98 (0.92)	1.00 (0.99)
Multiplicity	3.7 (3.7)	3.7 (3.7)	7.3 (6.5)	9.1 (9.0)
CC 1/2	0.998 (0.749)	0.995 (0.543)	0.997 (0.96)	0.998 (0.365)
Refinement				
Resolution range (Å)	32.25–1.85 (1.92–1.85)	41.41–1.95 (2.02–1.95)	48.25–2.49 (2.58–2.49)	44.69–1.60 (1.66–1.60)
Total reflections	128,237 (12,444)	194,082 (18,150)	96,661 (7,870)	451,600 (43,474)
Unique reflections	34,486 (3,389)	52,409 (4,966)	13,253 (1,217)	49,543 (4,833)
R-work	0.1693 (0.3087)	0.1933 (0.3101)	0.2489 (0.3388)	0.1639 (0.3570)
R-free	0.2104 (0.3415)	0.2397 (0.3851)	0.3082 (0.4382)	0.1997 (0.4065)
Number of Atoms				
Protein/Peptide	2,872	5,344	2,827	3,099
Ligands	36	100	12	36
Solvent	211	415	37	433
Average B-Factor				
Protein/Peptide	46.40	36.03	47.76	24.39
Ligands	47.09	51.09	63.94	27.50
Solvent	51.45	42.56	42.79	36.70
Root-Mean-Square Deviations				
Bond lengths (Å)	0.006	0.007	0.002	0.007
Bond angles (°)	0.74	0.79	0.47	0.91
Ramachandran				
Favored (%)	99	98	98	99
Outliers (%)	0	0	0.6	0

Numbers in parentheses refer to outer-shell statistics.

rational design of modulators of the pathway. Although the Bak core/latch dimer is not thought to form in physiological contexts, it provides a stable interface for *in vitro* BH3 peptide binding. We exploited this dimeric form as a tool for structural studies of Bak-BH3 peptide complexes. Crystal structures presented here provide details of Bim bound to this form of Bak that are consistent with previous biochemical and mutagenesis studies (Leshchiner et al., 2013; Letai et al., 2002), highlighting an important role for binding to the Bak hydrophobic groove.

A potential explanation for the apparent tighter affinity of Bim-BH3 for the core/latch dimer compared to monomeric Bak rests with the pre-exposure of Bak L100 to engage h0 residues on the peptide. Further validation of the importance of h0 residues engaging L100 is found in the 65-fold increase in affinity of Bim-h0-h3Glt (containing two Ile residues at h0) compared to Bim-h3Glt and the 100-fold loss of affinity of Bim-h0-h3Glt toward Bak L100A. The structures presented here reveal the key salt bridge that is observed in all other BH3:Bcl-2 protein interactions, but was absent in the majority of the 20 lowest-energy NMR structures of Bak in complex with a stapled Bid-BH3 peptide (Moldoveanu et al., 2013). Additionally, as the peptide(s) used in the current study did not require a hydrocarbon staple (between the h2 and h3 positions) to promote helicity and binding to Bak, our structures exclude possible additional interactions that occur between the staple and the groove in the Bak complex (in particular Bak Y89) (Moldoveanu et al., 2013).

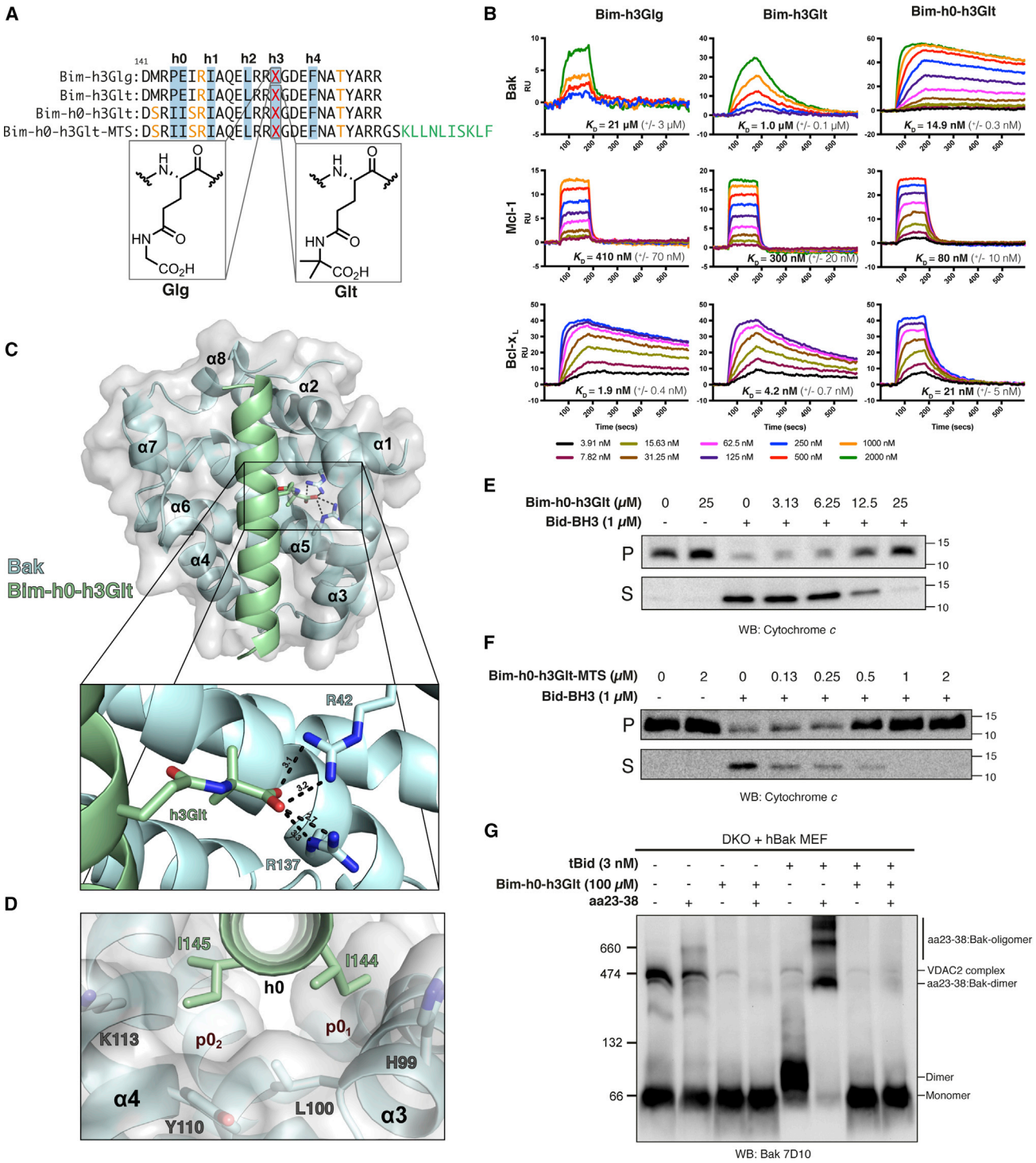

Figure 5. Inhibition of Bak Activation at the Mitochondria

(A) Sequence alignment of inhibitor peptides with conserved hydrophobic moieties highlighted (light blue), mutations to increase solubility shown in orange, artificial amino acids labeled with an X (red), mitochondrial targeting sequence (MTS) in green, and their chemical structure shown below.

(B) Surface plasmon resonance sensorgrams for Bim-h3Glg, Bim-h3Glt, and Bim-h0-h3Glt peptides binding to Bak, Mcl-1, and Bcl-x_L. Data are representative of the three independent experiments (KD values are mean ± SD).

(C) Crystal structure of Bim-h0-h3Glt (pale green) bound to Bak (pale cyan). The Glt side chain makes charge-charge interactions with R42 and R137 in Bak.

(D) The h0 moiety (I144 and I145) in Bim-h0-h3Glt (pale green) straddles the L100 residue in Bak (cartoon, pale cyan; surface, gray) and binds into two p0 pockets ($p0_1$ and $p0_2$) at the base of the hydrophobic groove.

(legend continued on next page)

The introduction of non-natural amino acids at the h3 position of Bim-RT, designed to displace solvent molecules from the p3 pocket and to create charge-charge interactions to Bak residues R42 and R137, resulted in peptides with increased affinity, to the point where complexes with monomeric Bak could be formed without the need for detergents such as CHAPS or hydrocarbon staples on the peptide. Importantly, this stabilized interaction converts BH3 peptides from Bak activators to Bak inhibitors. Inhibition of Bak activity might arise either through failure to trigger Bak-activating conformation changes or inhibiting the formation of the BH3-in-groove homodimer. Our structural and biochemical data indicate that inhibition was due to blockade of an early step in Bak conformation change. Interestingly, the additional interactions made by inhibitory peptides as compared to activating peptides included charge-charge interactions with R42 on helix α1. In contrast, few if any significant contacts were observed between the inhibitory (or activating) peptides and the latch domain at α8. Interaction with R42 in the α1 appears particularly important, because Bim-h3Pc-RT and Bim-h0-h3Glt peptides did not block activation of mBak where the corresponding residue is a leucine (L40), suggesting that these interactions may directly stabilize α1 to prevent its induced exposure during Bak activation (Griffiths et al., 1999). When this key residue is mutated in mBak (L40R), the capacity of Bim-h0-h3Glt to inhibit the protein is restored, demonstrating the specificity and mechanism of action of the inhibitor. Tethering α1 to either the core or latch domain prevents membrane permeabilization (Alsop et al., 2015). A recent study has also shown that antibodies that bind near the C terminus of α1 to displace it from the core of the protein can activate Bak (Iyer et al., 2016). Our structural data provide a rationale for the key role of the α1 dissociation as an early and requisite event in Bak activity.

What are the key sequence and structural features of the pro-apoptotic Bak and Bax, as compared to pro-survival proteins that render the former conformationally labile after transient interaction with activating BH3 peptides? The data presented here show that Bim-BH3 binds to Bak, Bax, and Bcl-x_L through similar interactions. However, significant differences exist between the structures of these complexes, most notably cavities present in Bak (Figure 1C) and Bax (Czabotar et al., 2013), but not in Bcl-x_L. Crystal structures of Bax bound to Bid-BH3, Bax-BH3 (Czabotar et al., 2013), or Bim-BH3 (Robin et al., 2015) all possess a cavity ~140 $Å^3$ in size located in the hydrophobic core of Bax between helices α1, α2, α5, and α8. In contrast, the cavity observed in Bak is much larger (351–435 $Å^3$), solvent filled, and in a different position (between the Bim-BH3 and Bak α1, α2, α3, and α5 helices) than those observed in the Bax:BH3 structures. Many structures of pro-survival Bcl-2 proteins in complex with BH3-peptides have been solved (Kvansakul and Czabotar, 2016), yet none of them possess significant cavities. Cavities have been reported to destabilize other proteins (Baase et al., 2010), and the cavity in Bax could be responsible for destabilizing the protein and promoting the conformation changes necessary for oligomerization (Czabotar et al., 2013). The solvent-filled space observed in the Bak:Bim-RT complex may play a similar role.

Relatively high concentrations of Bim-h0-h3Glt (25 μM), compared to its KD for Bak (15 nM), were required to inhibit cytochrome *c* release on isolated mitochondria. One explanation may be that only a small amount of Bak need be activated to induce cytochrome *c* release, whereas the vast majority of Bak molecules need to be blocked to inhibit all MOMP. Another explanation may lie in localization, similar to the increased potency observed for tBid compared to the Bid-BH3 alone (Hockings et al., 2015). The addition of a MTS to the inhibitor peptide significantly increased potency in these assays, confirming localization as a critical factor for inhibition.

Blue native page experiments revealed that Bak does not undergo activating conformational changes consistent with activation when the inhibitor peptide is bound. This indicates a stable complex has formed, which is consistent with our hypothesis for the mechanism of action of the inhibitor peptide (summarized in Figure 6). Interestingly, Bak was no longer observed in the higher-order complex that contains VDAC2 upon treatment with Bim-h0-h3Glt alone. This suggests that binding of an agent to the Bak groove is sufficient for dissociation of Bak from this complex. This may be because the groove itself interacts with VDAC2 or might result from allosteric effects induced by the opening of the groove upon peptide binding.

Recently designed BH3-mimetics that induce apoptosis have significant potential in the treatment of a variety of cancers (Ashkenazi et al., 2017; Lessene et al., 2013; Oltersdorf et al., 2005; Souers et al., 2013). However, little progress has been made in developing specific inhibitors of apoptosis. Genetic models have established a benefit to blocking the intrinsic apoptosis pathway in several disease models, including acute stress-related injuries to organs such as the kidney and liver (Wei et al., 2013), sepsis (Hotchkiss et al., 1999), hearing loss (Someya and Prolla, 2010), and ischemic reperfusion injury (Chen et al., 2001). While caspase inhibitors block apoptosis, they act downstream of the irreparable damage to the mitochondria and so do not confer long-term protection (van Delft et al., 2010). In contrast, inhibition of Bak (and/or Bax) to prevent mitochondrial disruption may provide a more effective strategy to inhibit cell death.

(E) Cytochrome *c* release assay on isolated mitochondria from DKO (*Bak*$^{-/-}$*Bax*$^{-/-}$) MEFs expressing human Bak. Increasing concentrations (μM) of the inhibitor peptide Bim-h0-h3Glt decreased cytochrome *c* release from the mitochondrial pellet (P) to the supernatant (S).
(F) Addition of a MTS to the Bim-h0-h3Glt peptide increased potency in cytochrome *c* release assays approximately 50-fold compared to (E) (for example, 0.5 μM of Bim-h0-h3Glt-MTS inhibited cytochrome *c* release to comparable levels observed with 25 μM of Bim-h0-h3Glt).
(G) Blue Native PAGE analysis of hBak inhibition by Bim-h0-h3Glt on isolated mitochondria from DKO (*Bak*$^{-/-}$*Bax*$^{-/-}$) MEFs expressing hBak. Bim-h0-h3Glt disrupted the association of Bak with a complex that contains VDAC2 and blocked tBid-induced dimerization of hBak. A conformation-specific Bak antibody (aa 23–38) binds to activated Bak and higher-order complexes (aa 23–38:Bak-dimer and aa23–38:Bak-oligomer) on Blue Native PAGE. These higher-order complexes were not observed in the presence of Bim-h0-h3Glt, indicating that the peptide had blocked both activation (exposure of the α1 helix) and dimerization.
Western blots in (E), (F), and (G) are representative of three independent experiments. See also Figure S6 and Tables 2 and S1.

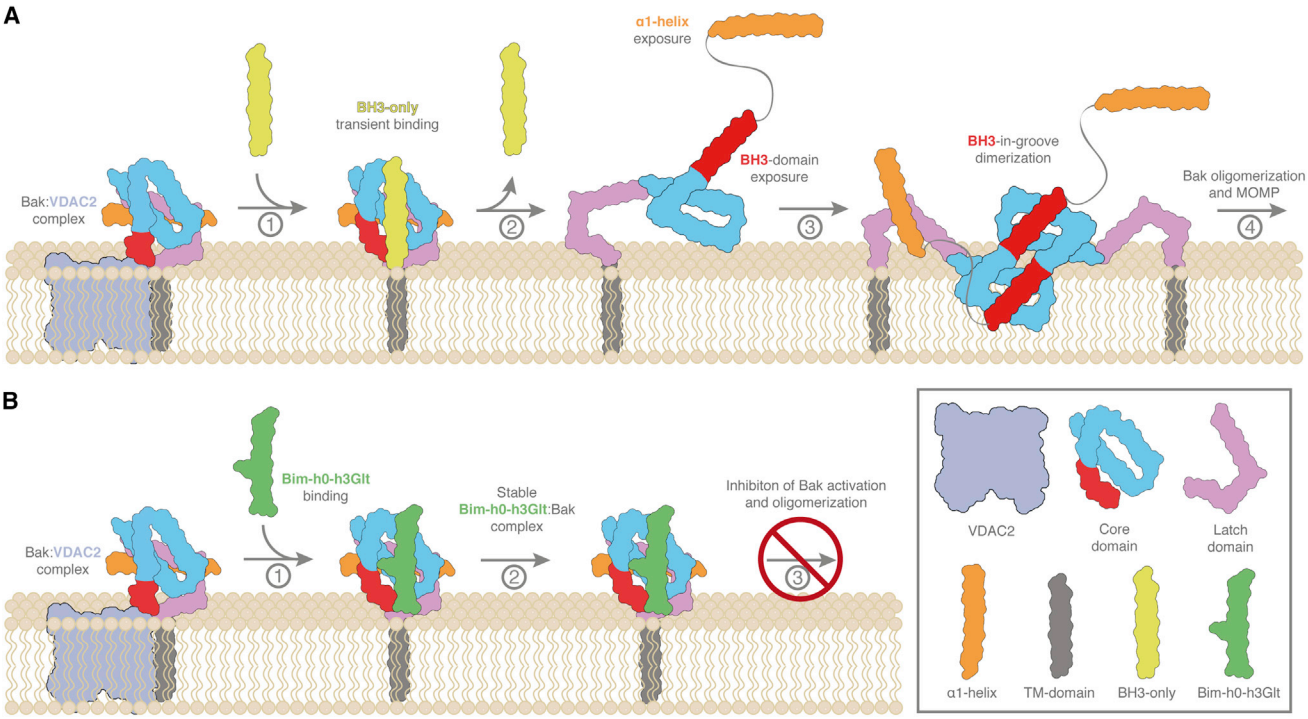

Figure 6. Schematic of Bak Activation and Inhibition at the Mitochondrial Outer Membrane

(A) Bak resides in the outer mitochondrial membrane in a complex that contains VDAC2. (1) Certain BH3-only proteins can directly interact with the hydrophobic groove of Bak, leading to its dissociation from this complex. (2) BH3-only protein binding is transient and causes conformation changes to occur in Bak, including release of the α1 helix, core/latch separation, and exposure of the BH3 domain. (3) Activated Bak molecules form symmetric BH3-in-groove dimers through core:core interactions. (4) Bak dimers are the building blocks for larger oligomers, which induce MOMP.

(B) (1) Bim-h0-h3GIt disrupts interactions between Bak and the VDAC2-containing complex by binding to the hydrophobic groove and α1 helix of Bak. (2) The Bim-h0-h3GIt peptide interacts directly with the Bak α1 helix, preventing its release and the subsequent core:latch separation and BH3 domain exposure. (3) By occluding the binding site for activators and blocking conformation changes, Bim-h0-3GIt inhibits Bak activation, oligomerization, and subsequent MOMP.

STAR★METHODS

Detailed methods are provided in the online version of this paper and include the following:

- KEY RESOURCES TABLE
- CONTACT FOR REAGENT AND RESOURCE SHARING
- EXPERIMENTAL MODEL AND SUBJECT DETAILS
- METHOD DETAILS
  - Recombinant Protein Expression and Purification
  - Crystallography
  - Cavity identification
  - Structural alignment
  - Gel filtration Dimerization Assay
  - Peptide Synthesis
  - Surface Plasmon resonance
  - Liposome release assay
  - Molecular modeling
  - Cytochrome *c* release assay
  - Blue Native PAGE
  - Chemical synthesis and analysis of artificial amino acids
- QUANTIFICATION AND STATISTICAL ANALYSIS
  - Determination of *KD*
  - Liposome release assay
- DATA AND SOFTWARE AVAILABILITY
- ADDITIONAL RESOURCES

SUPPLEMENTAL INFORMATION

Supplemental Information includes six figures, one table, and one dataset and can be found with this article online at https://doi.org/10.1016/j.molcel.2017.11.001.

AUTHOR CONTRIBUTIONS

Conceptualization, J.M.B., P.E.C., P.M.C., G.L., P.L.; Methodology, J.M.B., P.E.C., P.M.C., G.L., P.L., E.F.L., W.D.F.; Investigation, J.M.B., P.L., A.D.C., J.P.B., R.W.B., M.F.v.D., B.E.S., A.Y.R., A.W., I.K.T., M.J.C., B.J.S.; Resources, B.R.; Writing – Original Draft, J.M.B.; Writing – Review & Editing, J.M.B., P.E.C., P.M.C., G.L., G.D.; Funding Acquisition, P.E.C., P.M.C., G.L., J.M.B.; Supervision, P.E.C., P.M.C., G.L.

ACKNOWLEDGMENTS

We thank Janet Newman and colleagues at the CSIRO C3 crystallization facility; Matthew Call for discussions; Jai Rautela, Mike Ryan, David Huang, David Segal, Sweta Iyer, and Michael Dengler for reagents and technical assistance;

and Natasha Ritchie for proofreading the manuscript. This research was undertaken in part using the MX1 and MX2 crystallography beamlines at the Australian Synchrotron, Victoria, Australia, and made use of the ACRF Detector. P.E.C., G.L., and P.M.C. acknowledge NHMRC Fellowships (1079700, 1117089, 1116934). Our work is supported by NHMRC (Australia; Projects Grants 1079706 and 1059290 and Program Grant 1113133), the Australian Cancer Research Foundation, the Leukemia and Lymphoma Society (U.S.) (SCOR grant 7001-03), the Victorian State Government Operational Infrastructure Support, the Australian Government NHMRC IRIISS, and we acknowledge the support of the Walter and Eliza Hall Institute through the Catalyst Fund.

Received: May 26, 2017
Revised: September 15, 2017
Accepted: October 31, 2017
Published: November 16, 2017

REFERENCES

Adams, J.M., and Cory, S. (1998). The Bcl-2 protein family: arbiters of cell survival. Science *281*, 1322–1326.

Adams, P.D., Afonine, P.V., Bunkóczi, G., Chen, V.B., Davis, I.W., Echols, N., Headd, J.J., Hung, L.W., Kapral, G.J., Grosse-Kunstleve, R.W., et al. (2010). PHENIX: a comprehensive Python-based system for macromolecular structure solution. Acta Crystallogr. D Biol. Crystallogr. *66*, 213–221.

Alsop, A.E., Fennell, S.C., Bartolo, R.C., Tan, I.K., Dewson, G., and Kluck, R.M. (2015). Dissociation of Bak α1 helix from the core and latch domains is required for apoptosis. Nat. Commun. *6*, 6841.

Aluvila, S., Mandal, T., Hustedt, E., Fajer, P., Choe, J.Y., and Oh, K.J. (2014). Organization of the mitochondrial apoptotic BAK pore: oligomerization of the BAK homodimers. J. Biol. Chem. *289*, 2537–2551.

Ashkenazi, A., Fairbrother, W.J., Leverson, J.D., and Souers, A.J. (2017). From basic apoptosis discoveries to advanced selective BCL-2 family inhibitors. Nat. Rev. Drug Discov. *16*, 273–284.

Baase, W.A., Liu, L., Tronrud, D.E., and Matthews, B.W. (2010). Lessons from the lysozyme of phage T4. Protein Sci. *19*, 631–641.

Bleicken, S., Classen, M., Padmavathi, P.V., Ishikawa, T., Zeth, K., Steinhoff, H.J., and Bordignon, E. (2010). Molecular details of Bax activation, oligomerization, and membrane insertion. J. Biol. Chem. *285*, 6636–6647.

Bleicken, S., Jeschke, G., Stegmueller, C., Salvador-Gallego, R., García-Sáez, A.J., and Bordignon, E. (2014). Structural model of active Bax at the membrane. Mol. Cell *56*, 496–505.

Bombrun, A., Gerber, P., Casi, G., Terradillos, O., Antonsson, B., and Halazy, S. (2003). 3,6-dibromocarbazole piperazine derivatives of 2-propanol as first inhibitors of cytochrome c release via Bax channel modulation. J. Med. Chem. *46*, 4365–4368.

Brahmbhatt, H., Uehling, D., Al-Awar, R., Leber, B., and Andrews, D. (2016). Small molecules reveal an alternative mechanism of Bax activation. Biochem. J. *473*, 1073–1083.

Bricogne, G., Blanc, E., Brandl, M., Flensburg, C., Keller, P., Paciorek, W., Roversi, P., Sharff, A., Smart, O., Vonrhein, C., and Womack, T. (2011). BUSTER v.2.10.0 (Global Phasing Ltd.).

Brouwer, J.M., Westphal, D., Dewson, G., Robin, A.Y., Uren, R.T., Bartolo, R., Thompson, G.V., Colman, P.M., Kluck, R.M., and Czabotar, P.E. (2014). Bak core and latch domains separate during activation, and freed core domains form symmetric homodimers. Mol. Cell *55*, 938–946.

Certo, M., Del Gaizo Moore, V., Nishino, M., Wei, G., Korsmeyer, S., Armstrong, S.A., and Letai, A. (2006). Mitochondria primed by death signals determine cellular addiction to antiapoptotic BCL-2 family members. Cancer Cell *9*, 351–365.

Chen, Z., Chua, C.C., Ho, Y.S., Hamdy, R.C., and Chua, B.H. (2001). Overexpression of Bcl-2 attenuates apoptosis and protects against myocardial I/R injury in transgenic mice. Am. J. Physiol. Heart Circ. Physiol. *280*, H2313–H2320.

Chen, L., Willis, S.N., Wei, A., Smith, B.J., Fletcher, J.I., Hinds, M.G., Colman, P.M., Day, C.L., Adams, J.M., and Huang, D.C. (2005). Differential targeting of prosurvival Bcl-2 proteins by their BH3-only ligands allows complementary apoptotic function. Mol. Cell *17*, 393–403.

Czabotar, P.E., Lee, E.F., van Delft, M.F., Day, C.L., Smith, B.J., Huang, D.C., Fairlie, W.D., Hinds, M.G., and Colman, P.M. (2007). Structural insights into the degradation of Mcl-1 induced by BH3 domains. Proc. Natl. Acad. Sci. USA *104*, 6217–6222.

Czabotar, P.E., Lee, E.F., Thompson, G.V., Wardak, A.Z., Fairlie, W.D., and Colman, P.M. (2011). Mutation to Bax beyond the BH3 domain disrupts interactions with pro-survival proteins and promotes apoptosis. J. Biol. Chem. *286*, 7123–7131.

Czabotar, P.E., Westphal, D., Dewson, G., Ma, S., Hockings, C., Fairlie, W.D., Lee, E.F., Yao, S., Robin, A.Y., Smith, B.J., et al. (2013). Bax crystal structures reveal how BH3 domains activate Bax and nucleate its oligomerization to induce apoptosis. Cell *152*, 519–531.

Dai, H., Smith, A., Meng, X.W., Schneider, P.A., Pang, Y.P., and Kaufmann, S.H. (2011). Transient binding of an activator BH3 domain to the Bak BH3-binding groove initiates Bak oligomerization. J. Cell Biol. *194*, 39–48.

Dai, H., Pang, Y.P., Ramirez-Alvarado, M., and Kaufmann, S.H. (2014). Evaluation of the BH3-only protein Puma as a direct Bak activator. J. Biol. Chem. *289*, 89–99.

Dewson, G., Kratina, T., Sim, H.W., Puthalakath, H., Adams, J.M., Colman, P.M., and Kluck, R.M. (2008). To trigger apoptosis, Bak exposes its BH3 domain and homodimerizes via BH3:groove interactions. Mol. Cell *30*, 369–380.

Dewson, G., Ma, S., Frederick, P., Hockings, C., Tan, I., Kratina, T., and Kluck, R.M. (2012). Bax dimerizes via a symmetric BH3:groove interface during apoptosis. Cell Death Differ. *19*, 661–670.

Dorn, G.W., 2nd (2009). Apoptotic and non-apoptotic programmed cardiomyocyte death in ventricular remodelling. Cardiovasc. Res. *81*, 465–473.

Dundas, J., Ouyang, Z., Tseng, J., Binkowski, A., Turpaz, Y., and Liang, J. (2006). CASTp: computed atlas of surface topography of proteins with structural and topographical mapping of functionally annotated residues. Nucleic Acids Res. *34*, W116–118.

Emsley, P., and Cowtan, K. (2004). Coot: model-building tools for molecular graphics. Acta Crystallogr. D Biol. Crystallogr. *60*, 2126–2132.

Griffiths, G.J., Dubrez, L., Morgan, C.P., Jones, N.A., Whitehouse, J., Corfe, B.M., Dive, C., and Hickman, J.A. (1999). Cell damage-induced conformational changes of the pro-apoptotic protein Bak in vivo precede the onset of apoptosis. J. Cell Biol. *144*, 903–914.

Hanahan, D., and Weinberg, R.A. (2011). Hallmarks of cancer: the next generation. Cell *144*, 646–674.

Hetz, C., Vitte, P.A., Bombrun, A., Rostovtseva, T.K., Montessuit, S., Hiver, A., Schwarz, M.K., Church, D.J., Korsmeyer, S.J., Martinou, J.C., and Antonsson, B. (2005). Bax channel inhibitors prevent mitochondrion-mediated apoptosis and protect neurons in a model of global brain ischemia. J. Biol. Chem. *280*, 42960–42970.

Hockings, C., Anwari, K., Ninnis, R.L., Brouwer, J., O'Hely, M., Evangelista, M., Hinds, M.G., Czabotar, P.E., Lee, E.F., Fairlie, W.D., et al. (2015). Bid chimeras indicate that most BH3-only proteins can directly activate Bak and Bax, and show no preference for Bak versus Bax. Cell Death Dis. *6*, e1735.

Hotchkiss, R.S., Swanson, P.E., Knudson, C.M., Chang, K.C., Cobb, J.P., Osborne, D.F., Zollner, K.M., Buchman, T.G., Korsmeyer, S.J., and Karl, I.E. (1999). Overexpression of Bcl-2 in transgenic mice decreases apoptosis and improves survival in sepsis. J. Immunol. *162*, 4148–4156.

Hsu, Y.T., and Youle, R.J. (1997). Nonionic detergents induce dimerization among members of the Bcl-2 family. J. Biol. Chem. *272*, 13829–13834.

Iyer, S., Anwari, K., Alsop, A.E., Yuen, W.S., Huang, D.C., Carroll, J., Smith, N.A., Smith, B.J., Dewson, G., and Kluck, R.M. (2016). Identification of an activation site in Bak and mitochondrial Bax triggered by antibodies. Nat. Commun. *7*, 11734.

Jiang, M., Pabla, N., Murphy, R.F., Yang, T., Yin, X.M., Degenhardt, K., White, E., and Dong, Z. (2007). Nutlin-3 protects kidney cells during cisplatin therapy by suppressing Bax/Bak activation. J. Biol. Chem. *282*, 2636–2645.

Kabsch, W. (2010). Xds. Acta Crystallogr. D Biol. Crystallogr. *66*, 125–132.

Kluck, R.M., Bossy-Wetzel, E., Green, D.R., and Newmeyer, D.D. (1997). The release of cytochrome c from mitochondria: a primary site for Bcl-2 regulation of apoptosis. Science *275*, 1132–1136.

Kluck, R.M., Esposti, M.D., Perkins, G., Renken, C., Kuwana, T., Bossy-Wetzel, E., Goldberg, M., Allen, T., Barber, M.J., Green, D.R., and Newmeyer, D.D. (1999). The pro-apoptotic proteins, Bid and Bax, cause a limited permeabilization of the mitochondrial outer membrane that is enhanced by cytosol. J. Cell Biol. *147*, 809–822.

Korb, O., Stützle, T., and Exner, T.E. (2009). Empirical scoring functions for advanced protein-ligand docking with PLANTS. J. Chem. Inf. Model. *49*, 84–96.

Kotschy, A., Szlavik, Z., Murray, J., Davidson, J., Maragno, A.L., Le Toumelin-Braizat, G., Chanrion, M., Kelly, G.L., Gong, J.N., Moujalled, D.M., et al. (2016). The MCL1 inhibitor S63845 is tolerable and effective in diverse cancer models. Nature *538*, 477–482.

Ku, B., Liang, C., Jung, J.U., and Oh, B.H. (2011). Evidence that inhibition of BAX activation by BCL-2 involves its tight and preferential interaction with the BH3 domain of BAX. Cell Res. *21*, 627–641.

Kuwana, T., Bouchier-Hayes, L., Chipuk, J.E., Bonzon, C., Sullivan, B.A., Green, D.R., and Newmeyer, D.D. (2005). BH3 domains of BH3-only proteins differentially regulate Bax-mediated mitochondrial membrane permeabilization both directly and indirectly. Mol. Cell *17*, 525–535.

Kvansakul, M., and Czabotar, P.E. (2016). Preparing Samples for Crystallization of Bcl-2 Family Complexes. Methods Mol. Biol. *1419*, 213–229.

Lazarou, M., Stojanovski, D., Frazier, A.E., Kotevski, A., Dewson, G., Craigen, W.J., Kluck, R.M., Vaux, D.L., and Ryan, M.T. (2010). Inhibition of Bak activation by VDAC2 is dependent on the Bak transmembrane anchor. J. Biol. Chem. *285*, 36876–36883.

Le Guilloux, V., Schmidtke, P., and Tuffery, P. (2009). Fpocket: an open source platform for ligand pocket detection. BMC Bioinformatics *10*, 168.

Lee, E.F., Sadowsky, J.D., Smith, B.J., Czabotar, P.E., Peterson-Kaufman, K.J., Colman, P.M., Gellman, S.H., and Fairlie, W.D. (2009). High-resolution structural characterization of a helical alpha/beta-peptide foldamer bound to the anti-apoptotic protein Bcl-xL. Angew. Chem. Int. Ed. Engl *48*, 4318–4322.

Lee, E.F., Grabow, S., Chappaz, S., Dewson, G., Hockings, C., Kluck, R.M., Debrincat, M.A., Gray, D.H., Witkowski, M.T., Evangelista, M., et al. (2016). Physiological restraint of Bak by Bcl-xL is essential for cell survival. Genes Dev. *30*, 1240–1250.

Leshchiner, E.S., Braun, C.R., Bird, G.H., and Walensky, L.D. (2013). Direct activation of full-length proapoptotic BAK. Proc. Natl. Acad. Sci. USA *110*, E986–E995.

Lessene, G., Czabotar, P.E., Sleebs, B.E., Zobel, K., Lowes, K.N., Adams, J.M., Baell, J.B., Colman, P.M., Deshayes, K., Fairbrother, W.J., et al. (2013). Structure-guided design of a selective BCL-X(L) inhibitor. Nat. Chem. Biol. *9*, 390–397.

Letai, A., Bassik, M.C., Walensky, L.D., Sorcinelli, M.D., Weiler, S., and Korsmeyer, S.J. (2002). Distinct BH3 domains either sensitize or activate mitochondrial apoptosis, serving as prototype cancer therapeutics. Cancer Cell *2*, 183–192.

Li, H., Zhu, H., Xu, C.J., and Yuan, J. (1998). Cleavage of BID by caspase 8 mediates the mitochondrial damage in the Fas pathway of apoptosis. Cell *94*, 491–501.

Lindsten, T., Ross, A.J., King, A., Zong, W.X., Rathmell, J.C., Shiels, H.A., Ulrich, E., Waymire, K.G., Mahar, P., Frauwirth, K., et al. (2000). The combined functions of proapoptotic Bcl-2 family members bak and bax are essential for normal development of multiple tissues. Mol. Cell *6*, 1389–1399.

Liu, X., Kim, C.N., Yang, J., Jemmerson, R., and Wang, X. (1996). Induction of apoptotic program in cell-free extracts: requirement for dATP and cytochrome c. Cell *86*, 147–157.

Llambi, F., Moldoveanu, T., Tait, S.W., Bouchier-Hayes, L., Temirov, J., McCormick, L.L., Dillon, C.P., and Green, D.R. (2011). A unified model of mammalian BCL-2 protein family interactions at the mitochondria. Mol. Cell *44*, 517–531.

Luo, X., Budihardjo, I., Zou, H., Slaughter, C., and Wang, X. (1998). Bid, a Bcl2 interacting protein, mediates cytochrome c release from mitochondria in response to activation of cell surface death receptors. Cell *94*, 481–490.

Ma, S., Hockings, C., Anwari, K., Kratina, T., Fennell, S., Lazarou, M., Ryan, M.T., Kluck, R.M., and Dewson, G. (2013). Assembly of the Bak apoptotic pore: a critical role for the Bak protein α6 helix in the multimerization of homodimers during apoptosis. J. Biol. Chem. *288*, 26027–26038.

McCoy, A.J., Grosse-Kunstleve, R.W., Adams, P.D., Winn, M.D., Storoni, L.C., and Read, R.J. (2007). Phaser crystallographic software. J. Appl. Cryst. *40*, 658–674.

Moldoveanu, T., Liu, Q., Tocilj, A., Watson, M., Shore, G., and Gehring, K. (2006). The X-ray structure of a BAK homodimer reveals an inhibitory zinc binding site. Mol. Cell *24*, 677–688.

Moldoveanu, T., Grace, C.R., Llambi, F., Nourse, A., Fitzgerald, P., Gehring, K., Kriwacki, R.W., and Green, D.R. (2013). BID-induced structural changes in BAK promote apoptosis. Nat. Struct. Mol. Biol. *20*, 589–597.

Nakano, K., and Vousden, K.H. (2001). PUMA, a novel proapoptotic gene, is induced by p53. Mol. Cell *7*, 683–694.

Niu, X., Brahmbhatt, H., Mergenthaler, P., Zhang, Z., Sang, J., Daude, M., Ehlert, F.G.R., Diederich, W.E., Wong, E., Zhu, W., et al. (2017). A Small-Molecule Inhibitor of Bax and Bak Oligomerization Prevents Genotoxic Cell Death and Promotes Neuroprotection. Cell Chem. Biol. *24*, 493–506.e5.

Oberstein, A., Jeffrey, P.D., and Shi, Y. (2007). Crystal structure of the Bcl-XL-Beclin 1 peptide complex: Beclin 1 is a novel BH3-only protein. J. Biol. Chem. *282*, 13123–13132.

Oltersdorf, T., Elmore, S.W., Shoemaker, A.R., Armstrong, R.C., Augeri, D.J., Belli, B.A., Bruncko, M., Deckwerth, T.L., Dinges, J., Hajduk, P.J., et al. (2005). An inhibitor of Bcl-2 family proteins induces regression of solid tumours. Nature *435*, 677–681.

Peixoto, P.M., Teijido, O., Mirzalieva, O., Dejean, L.M., Pavlov, E.V., Antonsson, B., and Kinnally, K.W. (2017). MAC inhibitors antagonize the pro-apoptotic effects of tBid and disassemble Bax / Bak oligomers. J. Bioenerg. Biomembr. *49*, 65–74.

Polster, B.M., Basañez, G., Young, M., Suzuki, M., and Fiskum, G. (2003). Inhibition of Bax-induced cytochrome c release from neural cell and brain mitochondria by dibucaine and propranolol. J. Neurosci. *23*, 2735–2743.

Puthalakath, H., Huang, D.C., O'Reilly, L.A., King, S.M., and Strasser, A. (1999). The proapoptotic activity of the Bcl-2 family member Bim is regulated by interaction with the dynein motor complex. Mol. Cell *3*, 287–296.

Rami, A., Bechmann, I., and Stehle, J.H. (2008). Exploiting endogenous anti-apoptotic proteins for novel therapeutic strategies in cerebral ischemia. Prog. Neurobiol. *85*, 273–296.

Remé, C.E., Grimm, C., Hafezi, F., Wenzel, A., and Williams, T.P. (2000). Apoptosis in the Retina: The Silent Death of Vision. News Physiol. Sci. *15*, 120–124.

Robin, A.Y., Krishna Kumar, K., Westphal, D., Wardak, A.Z., Thompson, G.V., Dewson, G., Colman, P.M., and Czabotar, P.E. (2015). Crystal structure of Bax bound to the BH3 peptide of Bim identifies important contacts for interaction. Cell Death Dis. *6*, e1809.

Seo, Y.W., Shin, J.N., Ko, K.H., Cha, J.H., Park, J.Y., Lee, B.R., Yun, C.W., Kim, Y.M., Seol, D.W., Kim, D.W., et al. (2003). The molecular mechanism of Noxa-induced mitochondrial dysfunction in p53-mediated cell death. J. Biol. Chem. *278*, 48292–48299.

Someya, S., and Prolla, T.A. (2010). Mitochondrial oxidative damage and apoptosis in age-related hearing loss. Mech. Ageing Dev. *131*, 480–486.

Souers, A.J., Leverson, J.D., Boghaert, E.R., Ackler, S.L., Catron, N.D., Chen, J., Dayton, B.D., Ding, H., Enschede, S.H., Fairbrother, W.J., et al. (2013). ABT-199, a potent and selective BCL-2 inhibitor, achieves antitumor activity while sparing platelets. Nat. Med. *19*, 202–208.

Subburaj, Y., Cosentino, K., Axmann, M., Pedrueza-Villalmanzo, E., Hermann, E., Bleicken, S., Spatz, J., and García-Sáez, A.J. (2015). Bax monomers form dimer units in the membrane that further self-assemble into multiple oligomeric species. Nat. Commun. *6*, 8042.

Tehranian, R., Rose, M.E., Vagni, V., Pickrell, A.M., Griffith, R.P., Liu, H., Clark, R.S., Dixon, C.E., Kochanek, P.M., and Graham, S.H. (2008). Disruption of Bax protein prevents neuronal cell death but produces cognitive impairment in mice following traumatic brain injury. J. Neurotrauma *25*, 755–767.

van Delft, M.F., Smith, D.P., Lahoud, M.H., Huang, D.C., and Adams, J.M. (2010). Apoptosis and non-inflammatory phagocytosis can be induced by mitochondrial damage without caspases. Cell Death Differ. *17*, 821–832.

Wang, H., Takemoto, C., Akasaka, R., Uchikubo-Kamo, T., Kishishita, S., Murayama, K., Terada, T., Chen, L., Liu, Z.J., Wang, B.C., et al. (2009). Novel dimerization mode of the human Bcl-2 family protein Bak, a mitochondrial apoptosis regulator. J. Struct. Biol. *166*, 32–37.

Wei, M.C., Lindsten, T., Mootha, V.K., Weiler, S., Gross, A., Ashiya, M., Thompson, C.B., and Korsmeyer, S.J. (2000). tBID, a membrane-targeted death ligand, oligomerizes BAK to release cytochrome c. Genes Dev. *14*, 2060–2071.

Wei, M.C., Zong, W.X., Cheng, E.H., Lindsten, T., Panoutsakopoulou, V., Ross, A.J., Roth, K.A., MacGregor, G.R., Thompson, C.B., and Korsmeyer, S.J. (2001). Proapoptotic BAX and BAK: a requisite gateway to mitochondrial dysfunction and death. Science *292*, 727–730.

Wei, Q., Dong, G., Chen, J.K., Ramesh, G., and Dong, Z. (2013). Bax and Bak have critical roles in ischemic acute kidney injury in global and proximal tubule-specific knockout mouse models. Kidney Int. *84*, 138–148.

Wiessner, C., Allegrini, P.R., Rupalla, K., Sauer, D., Oltersdorf, T., McGregor, A.L., Bischoff, S., Böttiger, B.W., and van der Putten, H. (1999). Neuron-specific transgene expression of Bcl-XL but not Bcl-2 genes reduced lesion size after permanent middle cerebral artery occlusion in mice. Neurosci. Lett. *268*, 119–122.

Willis, S.N., Chen, L., Dewson, G., Wei, A., Naik, E., Fletcher, J.I., Adams, J.M., and Huang, D.C. (2005). Proapoptotic Bak is sequestered by Mcl-1 and Bcl-xL, but not Bcl-2, until displaced by BH3-only proteins. Genes Dev. *19*, 1294–1305.

Willis, S.N., Fletcher, J.I., Kaufmann, T., van Delft, M.F., Chen, L., Czabotar, P.E., Ierino, H., Lee, E.F., Fairlie, W.D., Bouillet, P., et al. (2007). Apoptosis initiated when BH3 ligands engage multiple Bcl-2 homologs, not Bax or Bak. Science *315*, 856–859.

Yin, X.M., Wang, K., Gross, A., Zhao, Y., Zinkel, S., Klocke, B., Roth, K.A., and Korsmeyer, S.J. (1999). Bid-deficient mice are resistant to Fas-induced hepatocellular apoptosis. Nature *400*, 886–891.

Yu, J., Zhang, L., Hwang, P.M., Kinzler, K.W., and Vogelstein, B. (2001). PUMA induces the rapid apoptosis of colorectal cancer cells. Mol. Cell *7*, 673–682.

Zha, H., Aimé-Sempé, C., Sato, T., and Reed, J.C. (1996). Proapoptotic protein Bax heterodimerizes with Bcl-2 and homodimerizes with Bax via a novel domain (BH3) distinct from BH1 and BH2. J. Biol. Chem. *271*, 7440–7444.

STAR★METHODS

KEY RESOURCES TABLE

REAGENT or RESOURCE	SOURCE	IDENTIFIER
Antibodies		
Bak (aa23-38) Rabbit	Sigma	#B5897; RRID: AB_258581
Bak (7D10) Rat	WEHI in house Ab (gift from Kluck lab)	N/A
Bax (49F9) Rat	WEHI in house (gift from Huang lab)	N/A
BclXL (2H12) Mouse	BD	#551022; RRID: AB_394007
Mcl-1 (polyclonal) Rabbit	Rockland Antibodies	600-401-394; RRID: AB_2266446
HSP70 (N6) Mouse	WEHI in house (gift from Huang lab)	N/A
Cytochrome *c* (7H8.2C12) Mouse	BD	556433; RRID: AB_396417
VDAC2 (polyclonal) Rabbit	Gift from Mike Ryan, Monash University, Australia	N/A
Chemicals, Peptides and Recombinant Proteins		
Bak ΔN22, ΔC25, C166S	Brouwer et al., 2014	N/A
Bak L100A ΔN22, ΔC25, C166S	This paper	N/A
Bak ΔC25 C-term-His	This paper	N/A
mBak ΔC25 C-term-His	This paper	N/A
hBax Full-Length	Czabotar et al., 2013	N/A
Bcl-x_L no loop Δ27-82, ΔC25	Oberstein et al., 2007	N/A
Bcl-x_L ΔC25	This paper	N/A
m/h Mcl-1	Czabotar et al., 2007	N/A
tBid	Kluck et al., 1999	N/A
Caspase-8	BD PharMingen	#556481
Thrombin	Sigma-Aldrich	10602400001 ROCHE
Bid-BH3	MIMOTOPES	N/A
Bim-WT	MIMOTOPES	N/A
Bim-RT	MIMOTOPES	N/A
Bim-h3Pc	MIMOTOPES	N/A
Bim-h3Pc-RT	MIMOTOPES	N/A
Bim-h3Glg	MIMOTOPES	N/A
Bim-h3Glt	MIMOTOPES	N/A
Bim-h0-h3Glt	MIMOTOPES	N/A
Bim-h0-h3Glt-MTS	MIMOTOPES	N/A
Bim-4E	Chen et al., 2005	N/A
Deposited Data		
Crystal Structure of Bak core/latch dimer: Bim-RT (cubic)	This paper	PDB: 5VWV
Crystal Structure of Bak core/latch dimer: Bim-RT (tetragonal)	This paper	PDB: 5VWW
Crystal Structure of Bak L100A	This paper	PDB: 5VX1
Crystal Structure of Bak monomer: Bim-h3Pc	This paper	PDB: 5VWZ
Crystal Structure of Bak core/latch dimer: Bim-h3Pc-RT	This paper	PDB: 5VYW
Crystal Structure of Mcl-1: Bim-h3Pc-RT	This paper	PDB: 5VX2
Crystal Structure of Bcl-xL: Bim-h3Pc-RT	This paper	PDB: 5VX3

(*Continued on next page*)

Continued		
REAGENT or RESOURCE	SOURCE	IDENTIFIER
Crystal Structure of Bak core/latch dimer: Bim-h0-h3GIt	This paper	PDB: 5VXW
Crystal Structure of Bak monomer: Bim-h3GIg	This paper	PDB: 5VX0
Experimental Models: Cell Lines		
WT MEF cells	N/A	N/A
DKO (*Bak*$^{-/-}$, *Bax*$^{-/-}$) MEF cells	N/A	N/A
DKO (*Bak*$^{-/-}$, *Bax*$^{-/-}$) + hBak MEF cells	N/A	N/A
mBax$^{-/-}$ MEF cells	N/A	N/A
Recombinant DNA		
pGEX 6p3- Bak ΔN22, ΔC25, C166S	Brouwer et al., 2014	N/A
pGEX 6p3 - Bak L100A ΔN22, ΔC25, C166S	This paper	N/A
pTYB1 - Bak ΔC25 C-term-His	This paper	N/A
pTYB1 - mBak ΔC25 C-term-His	This paper	N/A
pTYB1 - hBax Full-Length	Czabotar et al., 2013	N/A
pGEX 6p3 - Bcl-x_L no loop Δ27-82, ΔC25	This paper	N/A
pGEX 6p3 - Bcl-x_L ΔC25	This paper	N/A
pGEX 6p3 – m/h Mcl-1	Czabotar et al., 2007	N/A
Software and Algorithms		
F-pocket	Le Guilloux et al., 2009	N/A
CASTp	Dundas et al., 2006	N/A
COOT	Emsley and Cowtan, 2004	N/A
PHENIX	Adams et al., 2010	N/A
PHASER	McCoy et al., 2007	N/A
XDS	Kabsch, 2010	N/A
BUSTER	Bricogne et al., 2011	N/A
CLC Drug Discovery Workbench	N/A	N/A
Prism 7	GraphPad	N/A

CONTACT FOR REAGENT AND RESOURCE SHARING

Further information and requests for resources and reagents should be directed to Dr. Peter Czabotar (czabotar@wehi.edu.au).

EXPERIMENTAL MODEL AND SUBJECT DETAILS

Mouse embryonic fibroblasts (MEFs) derived from wild-type C57BL/6 mice at E14.5 were transformed with SV40 large T as previously described (Willis et al., 2007). MEFs were maintained in Dulbecco's modified Eagle's medium (DMEM) supplemented with 10% fetal calf serum (FCS), 250 μM L-asparagine and 55 μM 2-mercaptoethanol. Cells were cultured in 10% CO2 at 37°C, and split at < 80% confluency during maintenance.

METHOD DETAILS

Recombinant Protein Expression and Purification

Bak ΔN22, ΔC25, C166S

Human Bak (ΔN22, ΔC25, C166S) was expressed in and purified from *E. coli* BL21 (DE3) cells as described in Brouwer et al. (2014). The Bak L100A mutant used for crystallography was expressed and purified using the same method. Bak-GST was expressed and purified using the same method; however, the protein was eluted from the GST column with 10 mM reduced glutathione instead of being cleaved with precision protease.

Human Bak and Mouse Bak ΔC25 C-term-His

Human Bak (ΔC25), human Bak L100A (ΔC25) or mouse Bak (mBak)(ΔC25) containing a C-terminal Histidine-tag (6xHis residues) were cloned into the pTYB1 vector. The respective plasmid was then transformed into BL21 (DE3) *E. coli* cells and grown to an OD (600 nm) of ~1.0 in Super Broth. 1 mM IPTG was added to the culture and the protein was overexpressed for 3 hr at 37°C. Cells were lysed in TSE (Tris Sodium EDTA) buffer (20 mM Tris pH 8.0, 500 mM NaCl, 1 mM EDTA) and the proteins were passed over a chitin binding column, washed with TSE buffer and then chemically cleaved with DTT (50 mM) on-column for 48 hr at 4°C. Proteins were further purified by gel filtration (Sup75 10/300) in TBS.

hBax Full-Length

Full-length human Bax was expressed in and purified from *E. coli* BL21 (DE3) using the pTYB1 vector as performed in Czabotar et al. (2013).

Bcl-x_L no loop Δ27-82, ΔC25

A construct of Bcl-x_L described in Oberstein et al. (2007) lacking the α1–α2 loop (Δ27-82) and TM domain (ΔC25) was cloned into the pGEX 6P3 vector and then transformed into BL21 (DE3) *E. coli* cells. Cultures were grown to an O.D. (600 nm) of ~1.0 in Luria Super Broth, and cooled for 1 hr at 4°C. 1 mM IPTG was added to the culture and the protein was expressed overnight at 18°C. Cells were lysed in GST buffer (100 mM Tris, 50 mM NaCl, 1 mM EDTA) passed over a GST column and washed with 20 column volumes of GST buffer. Bcl-x_L was cleaved from GST on column overnight at 4°C with precision protease (0.02 mg/mL) and then purified by gel filtration (Sup75 10/300) in TBS (Tris buffer solution, 100 mM Tris, 50 mM NaCl).

Bcl-x_L ΔC25

Bcl-x_L lacking its TM domain (ΔC25) was cloned into the pGEX 6P3 vector and then transformed into BL21 (DE3) *E. coli* cells and grown in Luria Super Broth. At an OD (600 nm) of ~1.0 cultures before 1 mM IPTG was added to induce protein expression for 3 hr at 37°C. Cells were lysed in GST buffer (100 mM Tris, 50 mM NaCl, 1 mM EDTA) passed over a GST column and washed with 20 column volumes of GST buffer. GST-Bcl-x_L was then eluted from the column using 10 mM reduced glutathione before being further purified by gel filtration (Sup200 10/300) in TBS.

m/h Mcl-1

A chimera of Mcl-1 containing residues 152-189 from mouse and 209-327 from human Mcl-1 was expressed in and purified from *E. coli* BL21 (DE3) using the pGEX 6p3 vector as performed in Czabotar et al. (2007). The GST-tag was cleaved on column to produce m/h-Mcl-1 for crystallization. GST-m/h-Mcl-1 used in surface plasmon resonance experiments was produced by eluting the protein from the column with 10 mM reduced glutathione before further purification using gel filtration (Sup200 10/300) in TBS.

tBid

Truncated human Bid (tBid) was produced using a similar method to that reported in Kluck et al. (1999). tBid was cloned into the pGEX4T-1 vector and transformed into BL21 (DE3) cells and cultures were grown in SB to an OD (600 nm) of ~0.6. GST-hBid expression was induced with 1 mM IPTG for 16 hr at 18°C. Cells were lysed in phosphate buffer saline (PBS) containing EDTA (1 mM), DTT (1mM), 0.5 mM PMSF, aprotinin (10 μg/mL), leupeptin (10 μg/mL) and lysozyme (1 mg/mL), and passed over a GST column before being washed with PBS containing EDTA (1 mM), aprotinin (10 μg/mL) and leupeptin (10 μg/mL). The GST-hBid was then incubated with thrombin (SIGMA-ALDRICH - 1 unit/50 mL) in thrombin cleavage buffer (TCB - 50 mM tris pH 8.0, 150 mM NaCl, 5 mM $CaCl_2$) overnight at 4°C. hBid was eluted from the column in TCB, concentrated and further purified by gel filtration (Sup75 10/300) in TBS containing 2 mM DTT. hBid was then cleaved with caspase-8 (BD PharMingen) at a 1:1 ratio in HEPES pH 7.4, KCl (80 mM) and DTT (10 mM), at 37°C for 4 hr to produce truncated Bid (tBid). Caspase 8 was not removed from the final stock of tBid as it does not cytochrome *c* release alone (Kluck et al., 1999).

Crystallography

Bak core/latch dimer: Bim-RT peptide

Recombinant Human Bak (ΔC25, ΔN22, C166S) at 100 μM was incubated with 1% CHAPS and 1 mM Bid-BH3 peptide for 1 hr at RT. The resulting dimer was purified by gel filtration (Sup75 10/300) in TBS and concentrated to 250 μM. Bim-RT peptide (W147R, Y153T) (Figure 2A) was added in a 5-fold molar excess before crystallization. Two different conditions both produced unique crystal forms and resulted in the determination of two distinct structures in different space groups:

(1) Cubic, $P4_132$ (Figure 1, Table 1). Bak:Bim-RT $P4_132$ crystals were grown at 8°C in 18% glycerol, 21.6% PEG (poly-ethylene glycol) 1500 and 0.5% ethyl acetate. Crystals were frozen directly in well solution and X-ray data were collected at the Australian Synchrotron (MX2) at 100 K. Images were processed with XDS (Kabsch, 2010) and the structure was solved by molecular replacement with PHASER (McCoy et al., 2007) searching for one globule of the apo Bak core/latch dimer (PDB: 4U2U). The asymmetric unit contains one half of the Bak:Bim-RT core/latch dimer. The final model was produced by rounds of building in COOT (Emsley and Cowtan, 2004) and refinement using PHENIX (Adams et al., 2010).

(2) Tetragonal, $P4_32_12$ (Figure S1, Table 1). Bak:Bim-RT $P4_32_12$ grew at 8°C in a 12.5% MPD (2-methyl-2,4-pentanediol), 38 mM imidazole pH 6.5, 12.5% PEG 1000, 12.5% PEG 3350, 30 mM sodium fluoride, 30 mM sodium iodide, 62 mM sodium MES pH 6.5 and 30 mM sodium bromide. Crystals were directly frozen in well solution and diffraction data were collected at the Australian Synchrotron (MX2) at 100 K. Data were processed with XDS (Kabsch, 2010) and the structure was solved by molecular replacement with PHASER (McCoy et al., 2007) searching for two globules of the Bak core/latch dimer

(PDB: 4U2U). This was followed by several rounds of building in COOT (Emsley and Cowtan, 2004) and refinement using BUSTER (Bricogne et al., 2011) and PHENIX (Adams et al., 2010). The asymmetric unit contained one Bak:Bim-RT dimer complex, half of which was well defined (Globule 1, Figure S1b) and the other half less so (Globule 2, Figure S1b). Therefore, NCS restraints were used to aid in the refinement of "Globule 2".

Bak L100A monomer

See also Figure S2G and Table 1. Bak L100A (ΔC25, ΔN22, C166S) at 400 μM crystallized in 1 M sodium malonate-malonic acid pH 7.0 and 10% DL-malate-MES-tris pH 9.0 at 8°C. Crystals were frozen in cryo-protectant of mother liquor solution containing 25% ethylene glycol. Diffraction experiments were carried on the MX2 beamline at the Australian Synchrotron at 100K. Data were processed using XDS (Kabsch, 2010) and molecular replacement using PHASER (McCoy et al., 2007) solved the structure by searching for 2 copies of a previously solved Bak monomer (PDB: 2IMT). Rounds of building in COOT (Emsley and Cowtan, 2004) were combined with PHENIX (Adams et al., 2010) refinements to complete the structure.

Bak monomer: Bim-h3Pc

See also Figure 3 and Table 1. Bak (ΔC25, ΔN22, C166S) at 250 μM was mixed with a 4-fold excess of Bim-h3Pc (WT Bim-BH3 backbone) peptide (dissolved in H_2O). The complex was crystallized at 8°C in a condition (10% PEG 20000, 20% PEG MME 550, 38 mM Imidazole pH 6.5, 20 mM ammonium acetate, 20 mM potassium sodium tartrate, 20 mM sodium formate, 62 mM sodium MES pH 6.5, 20 mM trisodium citrate, and 20 mM sodium oxamate) from the "Morpheus" screen available at the CSIRO C3 crystallization facility. Crystals were directly frozen in mother liquor and diffraction data were collected at the Australian Synchrotron (MX1) at 100K. XDS (Kabsch, 2010) was used to process data images and molecular replacement using PHASER (McCoy et al., 2007) solved the structure by searching for one globule of the Bak core/latch dimer bound to Bim-BH3 (PDB: 5VWV). Several rounds of building in COOT (Emsley and Cowtan, 2004) and refinement using PHENIX (Adams et al., 2010) produced the final structure.

Bak core/latch dimer: Bim-h3Pc-RT

See also Figure S4 and Table 1. Bak (ΔC25, ΔN22, ΔCys) at 100 μM was incubated with 1% CHAPS and 1 mM Bid-BH3 peptide for 1 hr at RT. The resulting dimer was purified by gel filtration (Sup75 10/300) in TBS, concentrated to 250 μM and a 4-fold molar excess of Bim-h3Pc-RT peptide (dissolved in H_2O) was added to the protein before crystal screening. The complex was crystallized at 4°C in 15.8% PEG 8000, 50 mM potassium dihydrogen phosphate, and 22.7% glycerol. Crystals were directly frozen in mother liquor and diffraction data were collected at the Australian Synchrotron (MX2) at 100K. Images were processed with XDS (Kabsch, 2010) and the structure was solved by molecular replacement using PHASER (McCoy et al., 2007) searching for 2 copies of a Bak:Bim-BH3 globule (PDB: 5VWV). The structure was finalized by multiple rounds of refinement using PHENIX (Adams et al., 2010) and building in COOT (Emsley and Cowtan, 2004).

Mcl-1: Bim-h3Pc-RT

See also Figure 4C and Table 2. Mouse/human Mcl-1 at 3 mg/ml was incubated with a 1.3-fold molar excess of Bim-h3Pc-RT peptide (dissolved in H_2O) prior to crystallization. Crystals of the complex were grown at 8°C in 20% PEG 3000, 100 mM trisodium citrate buffered with citric acid pH 5.5, then frozen in well solution supplemented with 20% ethylene glycol before data collection at the Australian Synchrotron (MX2) at 100K. Data frames were processed with XDS (Kabsch, 2010) and the structure was solved using molecular replacement in PHASER (McCoy et al., 2007) searching for two copies of m/h Mcl-1: Bim-BH3 complex (PDB: 2NL9). Rounds of building in COOT (Emsley and Cowtan, 2004) and refinement using PHENIX (Adams et al., 2010) were used to further refine the structure.

Bcl-x_L: Bim-h3Pc-RT

See also Figure 4C and Table 2. Bcl-xL (no loop) α1 domain swapped dimers were purified from gel filtration and concentrated to 3.5 mg/ml before being mixed with a 1.3-fold molar excess of Bim-h3Pc-RT peptide (dissolved in H_2O). The complex was crystalized at 20°C in 200 mM magnesium chloride, 20% PEG 6000, and 100 mM sodium MES pH 6. Crystals were frozen in well solution supplemented with 20% ethylene glycol and X-ray diffraction data were collected on the MX2 beamline at the Australian Synchrotron at 100K. Diffraction images were processed using XDS (Kabsch, 2010) and PHASER (McCoy et al., 2007) was used to solve the structure by molecular replacement searching for two copies of Bcl-x_L α1 domain swapped dimers bound to Bim-BH3 (mutated to all alanine residues) (PDB: 3FDL). Rounds of building and refinement using COOT (Emsley and Cowtan, 2004) and PHENIX (Adams et al., 2010) respectively were used to obtain the final model.

Bak monomer: Bim-h3Glg

See also Figure S6E and Table 2. Bak (ΔC25, ΔN22, C166S) at 250 μM was mixed with 4-fold excess of the Bim-h3Glg peptide (dissolved in H_2O). The complex was crystallized at 8°C in 200 mM magnesium chloride, 25% PEG 3350, and 100 mM bis-tris chloride (pH 6.5). Crystals were directly frozen in well solution supplemented with 20% ethylene glycol and diffraction data were collected at the Australian Synchrotron (MX2) at 100K. XDS (Kabsch, 2010) was used to diffraction images and molecular replacement was performed using PHASER (McCoy et al., 2007) solved the structure by searching for one globule of the Bak core/latch dimer bound to Bim-BH3 (PDB: 5VWV). Rounds of building in COOT (Emsley and Cowtan, 2004) followed by refinement using PHENIX (Adams et al., 2010) resulted in the final structure.

Bak core/latch dimer: Bim-h0-h3Glt

See also Figure 5C and Table 2. Bak (ΔC25, ΔN22, ΔCys) at 100 μM was dimerized by incubation with 1% CHAPS and 1 mM Bid-BH3 peptide at RT for 1 hr. The dimer was purified by gel filtration (Sup75 10/300) in TBS, concentrated to 300 μM and a 4-fold molar excess of Bim-h0-h3Glt peptide (dissolved in H_2O) was added to the protein before crystallization. Crystals grew at 8°C in 200 mM calcium acetate, 30% PEG 400 and 100 mM sodium acetate-acetic acid pH 5.0. Crystals were frozen in well solution using liquid nitrogen to 100 K and X-ray diffraction experiments performed using a Dectris Eiger 16M on the MX2 beamline at the Australian Synchrotron. Diffraction images were processed using XDS (Kabsch, 2010) and PHASER (McCoy et al., 2007) was used to solve the structure by molecular replacement searching for two copies of half of the Bak:Bim-RT cubic crystal structure (PDB: 5VWV). Rounds of building in COOT (Emsley and Cowtan, 2004) and refinement using PHENIX (Adams et al., 2010) provided the final model.

Cavity identification

The program F-pocket (Le Guilloux et al., 2009) was used to identify cavities described in Figures 1 and S1 and CASTp (Dundas et al., 2006) was used to measure their volume.

Structural alignment

All structural alignments were performed in COOT (Emsley and Cowtan, 2004) by SSM superimpose and the number of residues aligned and RMSD of those residues are quoted.

Gel filtration Dimerization Assay

Bak (ΔC25, ΔN22, C166S) core/latch dimers were induced by incubating the protein with BH3-peptides and the detergent CHAPS as previously described in Brouwer et al. (2014). BH3-peptides (Bim-RT, Bid-BH3 or Bim-h3Pc-RT) at a final concentration of 1 mM were incubated with Bak or Bak L100A (100 μM) in the presence of the detergent CHAPS (1%) for 1 hr at RT and then analyzed by size exclusion chromatography (S75 10/300 column in TBS). Bim-h3Pc-RT was incubated with Bak for 30 min prior to incubation for 1 hr with Bid-BH3 in order to test the capacity of the Bim-h3Pc peptide to block dimerization (Figure 2E, pink elution profile).

Peptide Synthesis

Peptides Bim-BH3, Bid-BH3 and Bim-h3Pc were purchased from Mimotopes (Notting Hill, VIC, Australia). HPLC and Mass spectrometry analysis of purified peptides are provided in the supplemental data.

Surface Plasmon resonance

Surface Plasmon resonance binding assays were performed using either a BIAcore 3000 (Figures 2B and 2C, 4B) or BIAcore 4000 (Figure 5) instruments in an SPR buffer (10 mM HEPES, 150 mM NaCl, 3.4 mM EDTA, 0.005% Tween-20, pH 7.4). Bim-h3Pc-RT, Bim-WT were immobilized on a CM5 sensor chip surface by amine coupling, along with a Bim-4E peptide (Chen et al., 2005) as a non-binding reference peptide for experiments on the BIAcore 4000. Bak (ΔC25, ΔN22, C166S), m/h-Mcl-1 (ΔC25) and Bcl-xL (ΔC25) proteins were reconstituted in SPR buffer at varying concentrations injected for 360 s with 100 s dissociation time. Sensorgrams were double referenced by subtracting the Bim-4E channel responses from Bim-h3Pc-RT and Bim-WT responses, and a blank SPR buffer only sample. BIAcore 4000 experiments a CM5 sensor chip was immobilized with Anti-GST anitbodies (GST capture kit, GE healthcare) by amine coupling according to manufacturer's instructions. GST-Bak (ΔC25, ΔN22, C166S), GST-m/h-Mcl-1 (ΔC25), GST-Bcl-xL (ΔC25), or GST-Bak L100A (ΔC25, ΔN22, C166S) were reconstituted in SPR buffer at 5 μg/mL. GST protein samples were captured with 180 s injections onto spot 1 or 5. The chip was then blocked with GST in SPR buffer at 5 μg/mL 180 s injection prior to injecting peptides. Bim-h3Glg, Bim-h3Glt or Bim-h0-3Glt were reconsititued into SPR buffer at varying concentrations and injected for 120 s with 400 s dissociation time. The sensor surface was regenerated with glycine buffer (10 mM glycine pH 2.1) between each cycle before repeating capture and sample injections. Sensorgrams were fitted to either a Langmuir specific 1 site binding model derive kinetic parameters or at equilibrium by one site specific binding model, to derive dissociation constants (KD).

Liposome release assay

Liposome assays were performed on C-terminally His-tagged Bak, Bak L100A or mBak as we are unable to express full-length recombinant proteins. Liposomes contained a combination of lipids that mimic the outer-mitochondrial membrane (46% phosphatidylcholine, 25% phosphatidylethanolamine, 11% phosphatidylinositol, 10% phosphatidylserine, and 8% cardiolipin encapsulating self-quenching 5(6)-carboxy-fluorescein) supplemented with 5% of a nickel chelating lipid (1,2-Dioleoyl-sn-Glycero-3-[N-(5-amino-1-carboxypentyl)iminodiacetic-acid)-succinyl] in order to recruit C-terminally His-tagged proteins to the membrane. Lipid mixes in chloroform and 0.01% butylated hydroxytoluene were dried under N_2 and then re-suspended in SUV (small unilamellar vesicle/liposome) buffer (10 mM HEPES pH 7.5, 135 mM KCl, 1 mM $MgCl_2$) which contained 50 mM 5(6)-carboxy-fluorescein. Liposomes were then extruded through a 100 nm pore size membrane and passed over a PD10 column to remove excess dye. Liposomes (4 μg/ml) were incubated with either Bak (ΔC25 C-term-His), mBak (ΔC25 C-term-His) or hBax (full-length) at a concentration of

150 nM and varying concentrations of Bim-h3Pc-RT peptide in SUV buffer for 60 min at room temperature. They were then challenged by varying concentrations of the Bid-BH3 or Bim-RT, a direct activator of all three proteins. In the case of Bak L100A (ΔC25 C-term-His) Bid-BH3 (at varying concentrations) was incubated with the protein for 60 min. 5(6)-carboxy-fluorescein is self-quenching and upon release from liposomes its fluorescence was measured by excitation at 485 nm and emission at 535 nm.

Molecular modeling

CLC Drug Discovery Workbench software (version 2.4.1) was used to minimize each peptide analog using the crystal structure of Bim-h3Pc peptide bound to Bak (PDB: 5VWZ). A 14Å radius binding site, centralized to binding region of Bim-h3Pc peptide to Bak, was setup for minimalization of the input ligand. The water molecules present in the X-ray crystal structure were retained for docking purposes. The input ligand was built into the program using the ligand designer and Bim-h3Pc peptide as a template. To minimalize the binding confirmation of the input ligand, CLC Drug Discovery Workbench uses a standard mode to determine the favorable binding poses, which detects various flexible ligand conformations while holding protein as rigid structure during docking. The default number of iterations was set at 500. The ligand binding interactions of the resulting minimalization were observed using the CLC Drug Discovery visualization tool and a score calculated. The $PLANTS_{PLP}$ docking score (Korb et al., 2009) is used in the CLC Drug Discovery Workbench software.

Cytochrome *c* release assay

Cytochrome *c* release assays were performed as described in Dewson et al. (2008) on either DKO (*Bax*$^{-/-}$, *Bak*$^{-/-}$) MEF cells, or DKO MEF cells stably expressing human Bak (hBak), or *mBax*$^{-/-}$ MEF cells, or TKO (*Bax*$^{-/-}$, *Bak*$^{-/-}$, *Bcl-x*$_L$$^{-/-}$) MEF cells stably expressing hBak. Isolated mitochondria were incubated with Bim-h3Pc-RT (5 μM) or Bim-h0-h3Glt (3.1 μM, 6.25 μM, 12.5 μM, 25 μM, or 50 μM) for 30 min at 30°C before the addition Bid-BH3 (1 or 1.5 μM), or the Mcl-1 inhibitor S63845 (20 μM), which was then incubated for a further 30 min at 30°C. Supernatant and pellet fractions were separated by centrifugation (13000 rpm, 5 min) and analyzed for presence of cytochrome *c* by immunoblotting.

Blue Native PAGE

DKO (*Bax*$^{-/-}$*Bak*$^{-/-}$) MEFs were harvested and permeabilized (10x10^6 cells/mL) in digitonin (0.025% w/v) with protease inhibitors and 10 mM DTT in MELB (20 mM HEPES (pH 7.5), 100 mM sucrose, 2.5 mM $MgCl_2$, 100 mM KCl) for 10 min on ice. Membrane fractions were obtained by centrifugation (15000 rpm, 5 min, 4°C) and re-suspended in MELB buffer with 100 μM Bim-h0-h3Glt for 30 min on ice. Samples were then incubated with 3 nM tBid at 30°C for 30 min. Where indicated samples were then incubated with 1.5 μg of the antibody aa23-38 (Sigma) for 30 min on ice. Samples were then solubilized in 1% digitonin in solubilization buffer (20 mM Bis Tris (pH 7.4), 50 mM NaCl, 10% glycerol (v/v)) with protease inhibitors and 10 mM DTT for 30 min on ice. Soluble fraction was then obtained by centrifugation (15000 rpm, 4°C, 5 min) and supplemented with 10x Blue Native loading dye (100 mM Bis Tris (pH 7.0), 500 mM 6-aminohexanoic acid, 5% Coomassie Brilliant Blue). Samples were run on BN-PAGE and transferred to PVDF and blocked with 5% (w/v) skim milk in TBS-T (Tris buffered Saline + Tween – 20 mM Tris pH 7.6, 137 mM NaCl, 0.1% Tween-20) before blotting for Bak with the antibody 7D10 as described in Ma et al. (2013). For VDAC2 blotting PVDF membrane was incubated for 2 hr with anti-VDAC2 polyclonal primary antibody diluted in TBS-T, washed for 30 min in TBS-T, incubated with HRP-conjugated anti-rabbit secondary antibody in TBS-T then washed again for 30 min before incubation with ECL reagent (GE Healthcare), developed according to manufacturers' instructions and exposed on the Chemidoc (Biorad).

Chemical synthesis and analysis of artificial amino acids

Unless otherwise specified, proton (^{1}H) and carbon (^{13}C) NMR spectra were recorded at room temperature in base-filtered $CDCl_3$ on a Bruker spectrometer operating at 300 MHz for proton and 75 MHz for carbon nuclei. For ^{1}H NMR spectra, signals arising from the residual protio-forms of the solvent were used as the internal standards. ^{1}H NMR data are recorded as follows: chemical shift (δ) [multiplicity, coupling constant(s) *J* (Hz), relative integral] where multiplicity is defined as: s = singlet; d = doublet; t = triplet; q = quartet; m = multiplet or combinations of the above. The signal due to residual $CHCl_3$ appearing at δ_H 7.26 and the central resonance of the $CDCl_3$ "triplet" appearing at δ_C 77.0 were used to reference ^{1}H and ^{13}C NMR spectra, respectively. Low-resolution ESI mass spectra were recorded on a single quadrupole liquid chromatograph-mass spectrometer, while high-resolution measurements were conducted on a time-of-flight instrument. Low- and high-resolution EI mass spectra were recorded on a magnetic-sector machine. Analytical thin layer chromatography (TLC) was performed on aluminum-backed 0.2 mm thick silica gel 60 F_{254} plates as supplied by Merck. Eluted plates were visualized using a 254 nm UV lamp and/or by treatment with a suitable dip followed by heating. These dips included phosphomolybdic acid: ceric sulfate: sulfuric acid (conc.): water (37.5 g: 7.5 g: 37.5 g: 720 mL) or potassium permanganate: potassium carbonate: 5% sodium hydroxide aqueous solution: water (3 g: 20 g: 5 mL: 300 mL). Flash chromatographic separations were carried out with silica gel 60 (40–63 μm) as the 3stationary phase and using the AR- or HPLC-grade solvents indicated. Starting materials and reagents were generally available from the Sigma–Aldrich, Merck, Combi-blocks, Ark-Pharm or Chem-Impex International Inc and were used as supplied. Where necessary, reactions were performed under a nitrogen atmosphere.

Compound 4

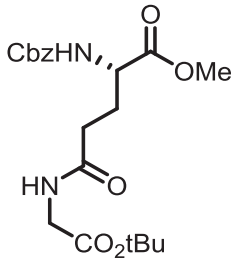

A magnetically stirred mixture of Cbz-Glu-OMe (1.20 g, 4.06 mmol) in DMF (12 mL) maintained at 18°C was treated with triethylamine (1.13 mL, 8.12 mmol) and HATU (2.30 g, 6.09 mmol), after stirring for 5 min, glycine *tert*-butyl ester hydrochloride 2 (0.82 g, 4.87 mmol) was added. The ensuing brown solution was stirred for 12 hr at 18°C before being poured onto $NaHCO_3$ (40 mL of a saturated aqueous solution) and extracted with EtOAc (50 mL). The separated organic phase was washed again with $NaHCO_3$ (40 mL of a saturated aqueous solution). The combined organic phases were washed with brine (100 mL), dried (Na_2SO_4), filtered and concentrated under reduced pressure. The residue thus obtained was subjected to chromatography (silica, 1:3 v/v EtOAc/hexane elution) to afford, after concentration of the relevant fractions (R_f = 0.4), *compound* 4 (1.38 g, 83%) as a colorless oil.

^{1}H NMR (300 MHz, $CDCl_3$) δ 7.37-7.30 (m, 5H), 6.29 (broad s, 1H), 5.74 (m, 1H), 5.10 (s, 2H), 4.41 (m, 1H), 3.90 (m, 2H), 3.73 (s, 3H), 2.38-2.16 (m, 3H), 2.04-1.92 (m, 1H), 1.46 (s, 9H).

^{13}C NMR (75 MHz, $CDCl_3$) δ 172.4, 171.8, 169.0, 156.2, 136.2, 128.5, 128.2, 128.1, 82.3, 67.0, 53.4, 52.5, 42.1, 32.0, 28.3, 28.0 (signals due to one carbon obscured or overlapping).

MS (ESI, +ev): *m/z* 431.2 ([M+Na] $^{+\bullet}$, 100%).

HRMS Calcd for $C_{20}H_{28}N_2O_7{}^{23}Na$: 431.1794. Found: 431.1797.

Compound Glg

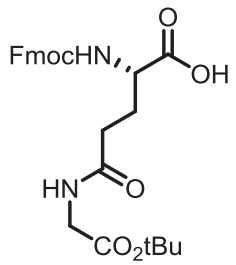

Step i: A flask was charged with compound 4 (1.30 g, 3.18 mmol), Palladium on carbon (0.13 g, 10% on carbon), and MeOH (40 mL). The atmosphere was flushed with hydrogen, and a balloon was attached. After being stirred at 18°C for 12 hr, the suspension was filtered through a pad of Celite, concentrated, the crude free amine was subjected to the next step directly.

Step ii: A magnetically stirred solution of above-mentioned crude product in methanol/water (50 mL of a 4:1 v/v mixture) was treated with LiOH (0.15 g, 6.36 mmol) and the ensuing mixture stirred at 18°C for 1 hr then concentrated under reduced pressure. The resulting crude amino acid was subjected to *step iii* directly.

Step iii: A magnetically stirred solution of above-mentioned crude product was dissolved in water (50 mL), the pH was adjusted to 9 by 1 M HCl, then a solution of FmocOSU (1.07 g, 3.18 mmol) in dioxane (20 mL) was added. The resulting solution was stirred at 18°C for 4 hr before being diluted with EtOAc (50 mL), the aqueous layer was separated and the pH was adjusted to 2 by 1 M HCl then extracted with EtOAc (2 × 50 mL). The combined organic layer was washed by brine (50 mL), dried (Na_2SO_4), filtered and concentrated under reduced pressure. The residue thus obtained was subjected to chromatography (silica, 5:95 v/v MeOH/CH_2Cl_2 elution) to afford, after concentration of the relevant fractions (R_f = 0.2), *compound* Glg (0.55 g, 36% from 4) as a white foaming solid.

^{1}H NMR (300 MHz, $CDCl_3$) δ 7.75 (m, 2H), 7.61 (m, 2H), 7.38 (m, 2H), 7.30 (m, 2H), 6.74 (m, 1H), 6.05 (m, 1H), 4.55-4.30 (m, 3H), 4.20 (m, 1H), 3.92 (m, 2H), 2.52-2.38 (m, 2H), 2.28-2.21 (m, 1H), 2.10-1.94 (m, 1H), 1.45 (s, 9H).

^{13}C NMR (75 MHz, $CDCl_3$) δ 173.8, 173.6, 172.1, 169.2, 168.9, 156.4, 143.8, 143.6, 141.27, 130.1, 127.7, 127.1, 125.1, 119.9, 82.9, 67.2, 53.4, 47.1, 42.3, 32.1, 28.5, 27.9, 25.4. (signals due to one carbon obscured or overlapping).

MS (ESI, +ev): *m/z* 505.2 ([M+Na] $^{+\cdot}$, 20%), 187.0 (10), 98.8 (28), 74.8 (30), 60.7 (100).
HRMS Calcd for $C_{26}H_{30}N_2O_7{}^{23}Na$: 505.1951. Found: 505.1951.

Compound 5

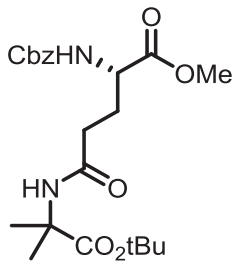

A magnetically stirred mixture of Cbz-Glu-OMe (3.0 g, 10.2 mmol) in DMF (30 mL) maintained at 18°C was treated with triethylamine (2.84 mL, 20.4 mmol) and HATU (5.82 g, 15.3 mmol), after stirring for 5 min, *tert*-butyl 2-amino-2-methylpropanoate hydrochloride 3 (1.95 g, 12.2 mmol) was added. The ensuing brown solution was stirred for 12 hr at 18°C before being poured into $NaHCO_3$ (100 mL of a saturated aqueous solution) and extracted with EtOAc (100 mL), the separated organic phase was washed again with $NaHCO_3$ (100 mL of a saturated aqueous solution). The combined organic phases were washed with brine (200 mL), dried (Na_2SO_4), filtered and concentrated under reduced pressure. The residue thus obtained was subjected to chromatography (silica, 1:3 v/v EtOAc/hexane elution) to afford, after concentration of the relevant fractions (R_f = 0.4), *compound* 5 (3.8 g, 85%) as a colorless oil.

^{1}H NMR (300 MHz, $CDCl_3$) δ 7.34-7.28 (m, 5H), 6.51 (broad s, 1H), 5.89 (dm, *J* = 9 Hz, 1H), 5.06 (s, 2H), 4.34 (m, 1H), 3.69 (s, 3H), 2.20-2.07 (m, 3H), 2.01-1.88 (m, 1H), 1.46 (s, 3H), 1.45 (s, 3H), 1.41 (s, 9H).

^{13}C NMR (75 MHz, $CDCl_3$) δ173.7, 172.4, 170.8, 156.2, 136.1, 128.3, 127.9(9), 127.9(4), 81.4, 66.8, 56.8, 53.5, 52.3, 32.5, 27.9, 27.7, 24.5, 24.3. (signals due to one carbon obscured or overlapping).

MS (ESI, +ev): *m/z* 459.2 ([M+Na] $^{+\cdot}$, 60%), 60.7 (100).
HRMS Calcd for $C_{22}H_{32}N_2O_7{}^{23}Na$: 459.2107. Found: 459.2106.

Compound Glt

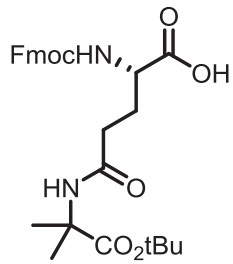

Step i: A flask was charged with compound **5** (3.8 g, 8.71 mmol), Palladium on carbon (0.38 g, 10% on carbon), and MeOH (100 mL). The atmosphere was flushed with hydrogen, and a balloon was attached. After being stirred at 18°C for 12 hr, the suspension was filtered through a pad of Celite, concentrated, the crude free amine was subjected to the next step directly.

Step ii: A magnetically stirred solution of above-mentioned crude product in methanol/water (100 mL of a 4:1 v/v mixture) was treated with LiOH (0.48 g, 17.42 mmol) and the ensuing mixture stirred at 18°C for 1 hr then concentrated under reduced pressure. The resulting crude amino acid was subjected to *step iii* directly.

Step iii: A magnetically stirred solution of above-mentioned crude product was dissolved in water (100 mL), the pH was adjusted to 9 by 1 M HCl, then a solution of FmocOSU (2.94 g, 8.71 mmol) in dioxane (40 mL). The resulting solution was stirred at 18°C for 4 hr before being diluted with EtOAc (100 mL), the aqueous layer was separated and the pH was adjusted to 2 by 1 M HCl then extracted with EtOAc (2 × 100 mL). The combined organic layer was washed by brine (100 mL), dried (Na_2SO_4), filtered and concentrated under reduced pressure. The residue thus obtained was subjected to chromatography (silica, 5:95 v/v MeOH/CH_2Cl_2 elution) to afford, after concentration of the relevant fractions (R_f = 0.2), *compound* Glt (1.5 g, 34% from 5) as a white foaming solid.

^{1}H NMR (300 MHz, $CDCl_3$) δ 7.75 (d, *J* = 9 Hz, 2H), 7.60 (dm, *J* = 9 Hz, 2H), 7.39 (t, *J* = 6 Hz, 2H), 7.30 (td, *J* = 7.4 and1.3 Hz, 2H), 6.83 (broad s, 1H), 6.07 (d, *J* = 6 Hz, 1H), 4.45-4.30 (m, 3H), 4.20 (t, *J* = 6 Hz, 1H), 2.51-2.29 (m, 2H), 2.24-2.15 (m, 1H), 2.10-1.95 (m, 1H), 1.52 (s, 3H), 1.51 (s, 3H), 1.45 (s, 9H).

^{13}C NMR (75 MHz, $CDCl_3$) δ 173.7, 173.4, 172.9, 171.9, 156.4, 143.8, 143.6, 141.2(8), 141.2(6), 127.7, 127.1, 125.1, 119.9, 82.2, 67.2, 57.4, 53.4, 47.1, 32.9, 28.9, 27.8, 25.4, 24.4, 24.2. (signals due to one carbon obscured or overlapping).

MS (ESI, +ev): *m/z* 533.2 ([M+Na] $^{+\cdot}$, 35%), 60.7 (100).

HRMS Calcd for $C_{28}H_{34}N_2O_7{}^{23}Na$: 533.2264. Found: 533.2260.

QUANTIFICATION AND STATISTICAL ANALYSIS

Determination of *KD*

Sensorgrams were fitted to either a Langmuir specific 1 site binding model derive kinetic parameters or at equilibrium by one site specific binding model, to derive dissociation constants (KD). Final quoted KD values derived from Figures 2B, 2C, 4B, and 5B are the mean from 3 independent experiments ± SD.

Liposome release assay

IC_{50} values were calculated in Prism 7 using non-linear regression to a sigmoidal dose response curve with a hill slope of −1.5, fitting to mean values from 3 independent experiments.

DATA AND SOFTWARE AVAILABILITY

The accession codes for the structures reported in this paper are PDB: 5VWV, 5VWW, 5VWX, 5VWY, 5VWZ, 5VX0, 5VX1, 5VX2, 5VX3.

ADDITIONAL RESOURCES

CLC Drug Discovery Workbench: https://www.qiagenbioinformatics.com/products/clc-main-workbench/

Prism 7: https://www.graphpad.com